Palaeogeography, Palaeoclimatology, Palaeoecology 511 (2018) 483–505

Contents lists available at ScienceDirect

Palaeogeography, Palaeoclimatology, Palaeoecology

journal homepage: www.elsevier.com/locate/palaeo

The palaeoceanographic crisis of the Early Aptian (OAE 1a) in the Vocontian Basin (SE France)

Fabienne Giraud[a,*], Bernard Pittet[b], Danièle Grosheny[c], François Baudin[d], Christophe Lécuyer[b,1], Tatsuhiko Sakamoto[e]

[a] Univ. Grenoble Alpes, Univ. Savoie Mont Blanc, CNRS, IRD, IFSTTAR, ISTerre, 38000 Grenoble, France
[b] Université de Lyon, UCBL, ENSL, CNRS, LGL-TPE, 69622 Villeurbanne, France
[c] Université de Lorraine, CNRS, CREGU, GeoRessources Lab, Faculté des Sciences et Technologies, 54506 Vandoeuvre-lès-Nancy, France
[d] Sorbonne Université, CNRS, ISTeP, 4 place Jussieu, 75005 Paris, France
[e] Mie University, 1577 Kurimamachiya-cho, Tsu City, Mie 514-8507, Japan

ARTICLE INFO

Keywords:
"Niveau Goguel"
Microfossils
Stable isotopes
Organic matter
Cyclostratigraphy
Carbonate production

ABSTRACT

The Vocontian Basin (SE France) which presents lower Aptian expanded successions characterized by major lithological changes, is particularly suitable to determine palaeoenvironmental changes occurring across the OAE 1a. A multidisciplinary study (sedimentology, $CaCO_3$, TOC, carbon and oxygen stable isotopes, micropalaeontology, cyclostratigraphy) was carried out in the Notre-Dame-de-Rosans section in order to establish a detailed chronological framework of these changes. The OAE 1a corresponds to carbon isotope segments C3–C6, and it lasted for 1.2 Myr. A first drop in the carbonate production occurs 500 kyr before the OAE 1a (upper part of the carbon isotope segment C2), and could result from both onset of "Urgonian" carbonate platform demise and associated reducing export of platform-derived sediments into the basin, and nannoconid crisis. A second drastic drop (crash) in the carbonate production is recorded within the lower part of the OAE 1a (latter part of segment C3 to C5) and is explained by a strong dissolution. This study then shows that the onset of the major carbonate crisis, that occurs before the OAE 1a, could be due to both rise in sea-level and in marine surface water fertility, whereas its "acme" that occurs within the OAE 1a, could be related to CO_2-induced ocean acidification. Black shales of the "Niveau Goguel" occur in the upper part of the OAE 1a and represent the lower part of segment C6. Surface-waters primary producers are principally represented by cyanobacteria, whereas nannofossil primary productivity is reduced, and deep-water anoxia prevailed during the deposition of "the Niveau Goguel". The last 300 kyr of the OAE 1a are characterized by a partial recovery of both nannofossil primary productivity and pelagic carbonate production, which sharply increase just after the end of the event. This study also shows that organic-rich layers associated to the OAE 1a are diachronous in the Tethyan realm.

1. Introduction

The Oceanic Anoxic Event (OAE) 1a (Early Aptian) was first described by Schlanger and Jenkyns (1976). This event is characterized by enhanced burial of organic matter, which is generally attributed to an increase in marine primary productivity under oceanic dysoxic/anoxic conditions which in turn lead to black shale deposits (Coccioni et al., 1992; Erba, 1994, Erba, 2004; Erbacher et al., 1996; Leckie et al., 2002; Jenkyns, 2010; Erba et al., 2015). A global perturbation in the carbon cycle is associated with this event; it is characterized by a major negative excursion up to 6‰ (C_{org}) recorded in both atmospheric and oceanic reservoirs (Jenkyns, 1995, 2010; Menegatti et al., 1998; Erba et al., 1999, 2015; Jahren et al., 2001; Bellanca et al., 2002; van Breugel et al., 2007), followed by a sharp shift towards more positive values. One possible explanation of the negative excursion is a volcanic episode of superplume that preceded the OAE 1a, corresponding to the formation of the Ontong-Java oceanic plateau (Larson and Erba, 1999; Méhay et al., 2009; Tejada et al., 2009; Bottini et al., 2012; Erba et al., 2015). This superplume could be responsible for an increase in atmospheric CO_2 (Jahren et al., 2001; Haworth et al., 2005; Hong and Lee, 2012; Naafs et al., 2016). The OAE 1a is also associated with major changes in carbonate production affecting both basinal and shallow-water settings (e.g. Erba, 1994, Erba and Tremolada, 2004; Weissert et al., 1998; Pittet et al., 2002; Weissert and Erba, 2004; Föllmi, 2012).

* Corresponding author.
E-mail address: Fabienne.Giraud-Guillot@univ-grenoble-alpes.fr (F. Giraud).
[1] Institut Universitaire de France.

https://doi.org/10.1016/j.palaeo.2018.09.014
Received 27 April 2018; Received in revised form 7 September 2018; Accepted 10 September 2018
Available online 15 September 2018
0031-0182/

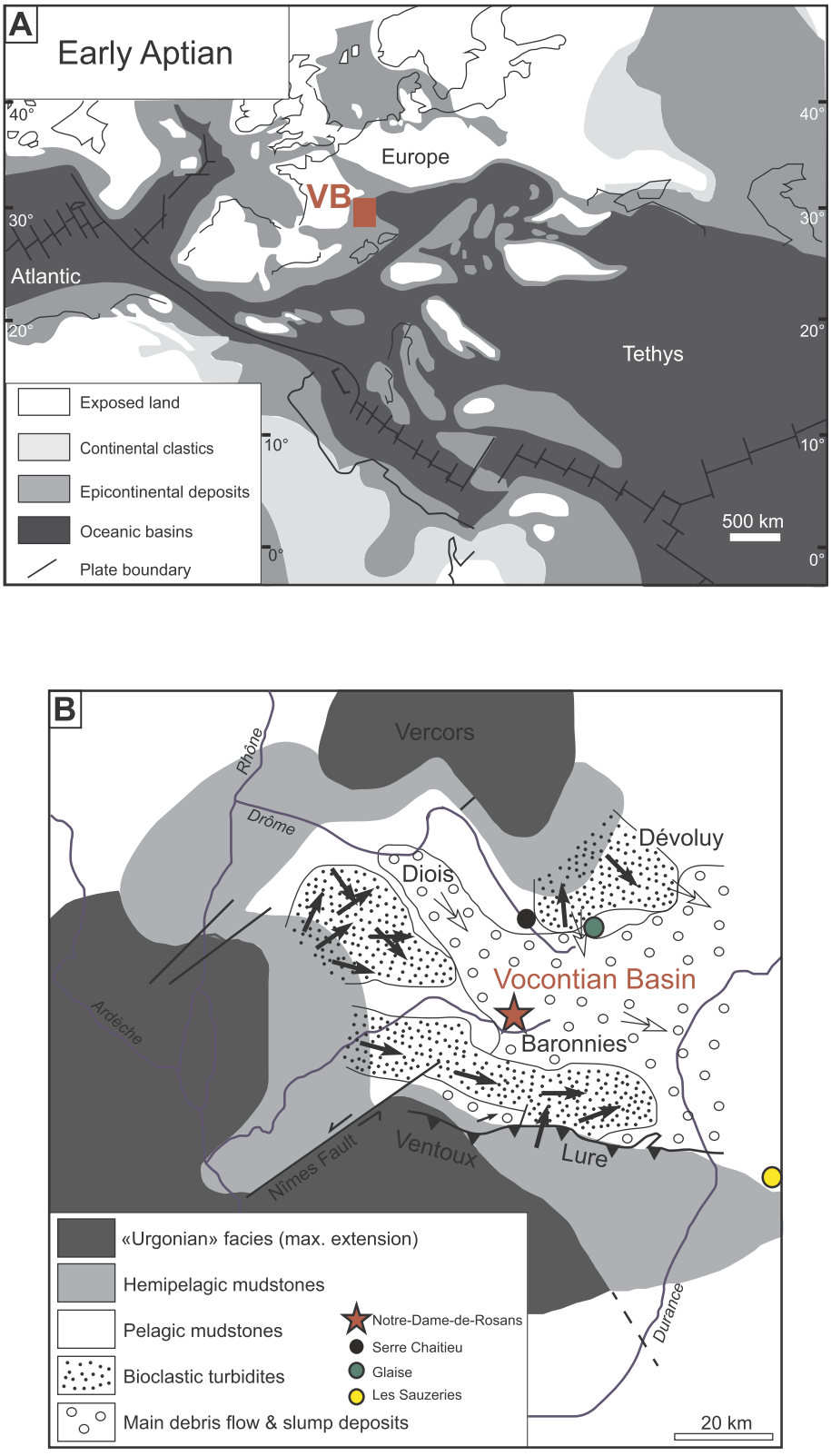

Fig. 1. A. Palaeogeographic map of the western Tethys and Central Atlantic Ocean in the Early Aptian, modified from Masse et al. (2000). B. Location of the Notre-Dame-de-Rosans section in the Vocontian Basin (Barremian/Aptian palaeogeography modified from Ferry and Rubino, 1989). The location of other Vocontian sections discussed in this study is indicated.

Some 40 kyr before the OAE 1a, calcareous phytoplankton assemblages recorded a nannoconid crisis (Erba, 1994, 1996; Erba et al., 2010; Malinverno et al., 2010). This crisis spanned the whole interval corresponding to the OAE 1a and a small recovery was observed after this event (Bralower et al., 1994, 1999; Erba, 1994; Erba et al., 1999; Erba and Tremolada, 2004). It corresponds to a reduction in biocalcification, and could be the result of a combined higher fertility (Coccioni et al., 1992; Erba, 1994; Erbacher et al., 1996; Cobianchi et al., 1999;

Premoli Silva et al., 1999; Leckie et al., 2002; Aguado et al., 2014) and higher atmospheric CO_2 during the superplume event, resulting in an acidification of marine waters (Erba and Tremolada, 2004; Erba et al., 2010; Erba et al., 2015). This scenario contrasts with the suggestions of previous authors who underlined that enhanced primary productivity and black shale deposits were synchronous. Most of the palaeoenvironmental interpretations inferred from the studies of OAE 1a presented above concern sections from pelagic and/or hemipelagic settings such as Cismon (southern Alps, Italy) and oceanic settings. Recently, Naafs et al. (2016) studied an expanded section in southern Spain and demonstrated that a significant time lag recorded between the onset of the nannoconid crisis and the onset of the CO_2 increase indicates that CO_2-induced surface ocean acidification did not cause the nannoconid biocalcification crisis.

A time calibration of the OAE 1a with carbon isotopes is generally reliable since correlations can be established between both onshore and offshore sections. A chemostratigraphy established for the first time with the $\delta^{13}C_{carb}$ record of the Cismon section by Menegatti et al. (1998), allowed the identification of different segments (C1 to C8) both on neritic and pelagic sections of the Tethyan margins and in Atlantic and Pacific oceanic settings. The OAE 1a starts with the carbon isotope segment C3 and ends within C6 as defined by Menegatti et al. (1998). Cyclostratigraphic analyses carried out on the Cismon APTICORE by Malinverno et al. (2010) and on various Tethyan sections as well as oceanic DSDP sites by Li et al. (2008) provide a duration comprised between 1.1 and 1.3 Myr for the OAE 1a. However, if we now consider the duration estimations of the segments identified by Menegatti et al. (1998), these estimations are rather different from one author to another, depending on the selected sections. In particular, the range duration observed for C3 is comprised between 22 and 47 kyr in the section of Cismon (Li et al., 2008; Malinverno et al., 2010), the Santa Rosa Canyon in Mexico and in the North Atlantic DSDP Site 398 (Li et al., 2008), whereas longer durations that range from 100 to 390 kyr are observed in more expanded sections (Glaise, Vocontian Basin, southeast France, Huck et al., 2011; La Bédoule, South Provençal Basin, southeast France, Kuhnt et al., 2011; Lorenzen et al., 2013; Yenicesihlar, central Turkey, Hu et al., 2012; Bab Basin, southern Arabian Gulf, Yamamoto et al., 2013). In the Cismon APTICORE, the segment C3 has recently been redefined, with an update duration comprised between 100 and 200 kyr (Bottini et al., 2015).

Thus, we consider necessary to investigate expanded sections to better depict the chronology of the main palaeoenvironmental changes across the OAE 1a (i.e., the carbonate crisis, enhanced primary productivity and black shale deposition among others) using a pluridisciplinary approach, and to better calibrate the duration of these environmental changes.

Lower Aptian deposits of the Vocontian Basin (SE France) record the OAE 1a (Bralower et al., 1994), represented by black shales deposits called the “Niveau Goguel” (Bréhéret, 1988). Some of the hemipelagic sections located in the central part of the basin are dilated and show the decrease in carbonate accumulation, recorded by abrupt changes in lithology, from lower Aptian limestone-marlstone alternations to marlstones including the “Niveau Goguel”. The purpose of this study was to investigate a lower Aptian expanded succession using a multidisciplinary approach (sedimentology, $CaCO_3$, TOC, carbon and oxygen stable isotopes, micropalaeontology, cyclostratigraphy) in order to establish a detailed chronological framework of the main palaeoenvironmental changes occurring across the OAE 1a. Detailed correlations of this framework with those of other Tethyan sections using litho-, bio- and chemostratigraphy are proposed.

2. Geological setting

The French Subalpine Basin, which is named the Vocontian Basin for the Cretaceous period, today constitutes a major segment of the southern subalpine ranges, and was located at a palaeolatitude of 25–30°N along the northwestern margin of the Tethys (Masse et al., 2000; Fig. 1A). It was surrounded by the “Urgonian” platforms: the Vercors platform northward, the Bas-Vivarais (Ardèche and Gard) platform westward, and the Provence platform southward (Cotillon et al., 1984). The structural framework of this basin reflected many tectonic phases related to the opening of the Bay of Biscay (Ricou and Frizon de Lamotte, 1986; Kandel, 1992; Hibsch et al., 1992). During the Tethyan rifting (Triassic to Lower Cretaceous), the French Subalpine Basin developed a major strike-slip fault system oriented N020° (Cévennes, Durance and Nîmes faults), which was inherited from the Hercynian phase (Masse and Philip, 1976). The Vocontian Basin was a subsiding and relatively deep marine area during the Early Cretaceous period (Fig. 1B). The lower Cretaceous hemipelagic deposits are thick (600 to 800 m), and mainly characterized by marlstone-limestone alternations forming continuous beds or units over the basin (Cotillon, 1971; Masse and Philip, 1976). The Late Barremian-Early Aptian interval is characterized by dominant calcareous limestone-marlstone alternations and followed by the lower Aptian-Albian Blue Marls Formation, up to 800 m thick (Flandrin, 1963; Friès, 1987; Bréhéret, 1997). Hence, an abrupt change in lithology occurred during the Early Aptian in the Vocontian Basin, and was related to a drastic drop in carbonate bioproductivity (Cotillon, 2010; Cotillon et al., 2000), possibly as a consequence of the nannoconid crisis; a crisis that was documented in southeastern France (Bergen, 1998). The Blue Marls Formation presents several black shale levels; the first of these levels has been named the “Niveau Goguel” (Bréhéret, 1988) and corresponds to the regional expression of the OAE 1a (Bralower et al., 1994). The decrease in carbonate accumulation includes the “Niveau Goguel”. The carbonate sedimentation recovered above the “Niveau Goguel”, and is characterized by a prominent lithostratigraphic horizon, called the “Niveau blanc” (Friès et al., 1984) and dated from the latest Early Aptian. This level is topped by the lowermost upper Aptian marlstones.

Previous studies of the OAE 1a were performed on different sections in the Vocontian Basin, but focused either on the “Niveau Goguel” only or were not based on a multidisciplinary approach. In the Serre Chaitieu section, located in the northwestern part of the basin, sedimentological ($CaCO_3$, clay minerals, spectral gamma ray, magnetic susceptibility), organic (TOC, biomarkers) and inorganic (carbon and oxygen stable isotopes) geochemical and micropalaeontological (calcareous nannofossils, palynomorphs and dinoflagellates) analyses were carried out (Bréhéret, 1997; Herrle and Mutterlose, 2003; Herrle et al., 2004; Heimhofer et al., 2004, 2006; Ghirardi et al., 2014). However, the study of Serre Chaitieu was devoted to the “Niveau Goguel” and sediments above and does not allow deciphering palaeoenvironmental changes prevailing at the onset of the OAE 1a. The Glaise section, located in the northeastern part of the basin, was studied for geochemistry (TOC, $\delta^{18}O$, $\delta^{13}C_{carb}$, $\delta^{13}C_{org}$, redox-sensitive trace-element (RSTE) distribution, phosphorus accumulation rates (PARs) and clay minerals (Stein et al., 2012; Westermann et al., 2013)). This section recovers the “Niveau Goguel” and sediments below and above, but any micropalaeontological data are available for the sediments above and below the “Niveau Goguel”. The last section is “Les Sauzeries”, located in the southeastern part of the basin, and was drilled. Only the “Niveau Goguel” was investigated in this section for geochemistry (TOC, biomarkers, $\delta^{13}C_{org}$, $\delta^{13}C_{carb}$, $\delta^{18}O$, $CaCO_3$; Okano et al., 2008; Ando et al., 2013).

The studied section of Notre-Dame-de-Rosans (geographical coordonates: Latitude 44°23′33 N/Longitude 05°29′58 E) is located on the departemental road 949, around 3 km to the northwest of the small locality Saint-André-de-Rosans belonging to the central part of the Vocontian Basin (southeast France; Fig. 1A–B). It provides a complete lower Aptian succession.

3. Material and methods

3.1. Sedimentology

The section has been described bed-by-bed. Lithology, texture, grain size and sedimentary structures (when present) have been analyzed in the field. Also, the marlstone color has been described as a first indication of the presence of organic carbon.

Bed organization and stacking pattern were observed along the section in order to define small lithological units (or sub-units) that may reflect cyclical changes in palaeoenvironmental conditions.

3.2. Calcareous nannofossils

Sixty-seven samples were collected all along the succession from favourable lithologies (calcareous clays, marlstones, argillaceous limestones) for nannofossil investigations, with a few number collected from limestones, in order to have a sampling representative of various lithologies.

Smear slides were prepared using the random settling technique developed by Geisen et al. (1999), a method adapted from Beaufort (1991), which allows the calculation of absolute abundances. Nannofossils were observed using light polarizing microscope, at 1560× magnification. In the richest samples, 500 specimens were generally counted in a variable number of fields of view. In the poorest samples, specimens were counted following one longitudinal transverse (200 fields of view). Observation of marker species was achieved by counting > 3 subsequent longitudinal transverses. All nannofossils with at least more than half of the specimen preserved were counted. The taxonomic frameworks of Perch-Nielsen (1985) and Bown et al. (1998) were followed. Nannofossil preservation was evaluated following the classes defined by Roth (1983). Nannofossil absolute abundances are usually biased by dilution. Therefore, nannofossil fluxes were calculated, using a cyclostratigraphy calibration made in this work (Section 5.1). Sedimentation rates were calculated for intervals corresponding to the small-scale lithological units of 100-kyr eccentricity cycles recognized (Fig. 2). Nannofossil fluxes are expressed as F (number of nannofossils/m^2/yr) = "AA × r × sed. rate" with AA = nannofossil absolute abundance, r = volume mass of calcite (2.7 g·cm^{-3}) and sed. rate = sedimentation rate. Sediment density is dependent on the composition and porosity of the rock; however, we demonstrated for Jurassic carbonate sediments with various calcium carbonate contents, that density has a low impact on flux calculation (Suchéras-Marx et al., 2014). Relative abundance of each species was also calculated for each sample. In this calculation, *Nannoconus* were excluded from the total sum of nannofossils because of their uncertain biological and ecological affinities (Aubry et al., 2005). Nannofossil assemblage composition was also described by means of species richness, the Shannon Diversity Index and evenness defined by Shannon and Weaver (1949). *Nannoconus* were excluded from these calculations as explained before.

3.3. Foraminifera

Foraminifera were studied from small-scale lithologic Units 8 to 15 on the basis of eighteen samples taken only in marlstones. Marly samples were put into a mixture of water and a small amount of 110 vol. hydrogen peroxide for 12 h, then washed using 1 mm and 63 µm meshes. Residues were dried at 40 °C. Material was well-preserved, preventing any problems with identification. Determinations were made using the systematics of Loeblich and Tappan (1988). The planktic zonal schemes used are those of Robaszynski et al. (1979), Caron (1985) and Robaszynski and Caron (1995). Residues lower than 63 µm were also examined. Foraminifera were identified and counted until a total of 250 specimens was reached, if possible. Several parameters were calculated such as the relative abundance of planktics (noted as planktics %), relative abundance of benthics (noted as benthics %), number of foraminifera per gram of sediment. Among benthics, percentages of suborders (Textularina, Rotalina, Lagenina) were also given.

3.4. Calcimetry and carbon and oxygen stable isotopes

Sixty-seven and forty-one samples corresponding to the different lithologies encountered all along the succession were analyzed for calcium carbonate content, and for stable carbon and oxygen ratios, respectively.

Calcium carbonate content was determined using the carbonate bomb technique, which measures CO_2 emission during a hydrochloric acid attack. The $CaCO_3$% was calculated using equations presented in Peybernès et al. (2013).

Stable isotope compositions of bulk samples were measured using a Multiprep™ automated preparation system coupled to a GV Isoprime® mass spectrometer at the Laboratoire de Géologie de Lyon (UMR 5276, Université Claude Bernard Lyon 1). For each sample, at least two aliquots of ≈300 to 500 µg were reacted with anhydrous oversaturated phosphoric acid at 90 °C during 20 min. Reproducibility of $\delta^{18}O$ measurements was 0.1‰ (1σ) and 0.05‰ (1σ) for $\delta^{13}C$. Data are reported as $\delta^{18}O$ and $\delta^{13}C$ values vs. VPDB (in ‰ δ units) following calibration with both limestone NIST NBS19 ($\delta^{13}C = +1.95$; $\delta^{18}O = -2.20$) and carbonatite NIST NBS18 ($\delta^{13}C = -5.01$; $\delta^{18}O = -23.00$) international standards according to the protocol given by Werner and Brand (2001).

3.5. Rock Eval

Total organic carbon content, thermal maturation and sources of the organic matter were estimated on 32 selected samples, using a Rock-Eval instrument, OSA device. The method, described in details by Espitalié et al. (1985-1986), consists in a two-step analysis with programmed temperature: a pyrolysis step operating under inert atmosphere (He), followed by an oxidation. Crushed samples are first subjected to a 3 min isotherm at 300 °C at which free hydrocarbons are volatilized (peak S1). Then, a heating with a ramp of 25 °C min^{-1} leads to the vaporization of products from thermal cracking of organic matter up to 600 °C (peak S2). Pyrolysis effluents are continuously detected by a flame ionization detector (FID) and expressed in mg per g of sample. At the end of the pyrolysis step, samples are automatically transferred into an oxidation oven where they are subjected to a 7 min isotherm at 600 °C. CO_2 generated by the oxidation of the remaining organic matter is detected by a catharometer and expressed in mg per g of sample. All those parameters allow the calculation of the total organic carbon (TOC) which is expressed as wt% of bulk rock samples. The hydrogen index (HI), corresponding to the quantity of hydrocarbon compounds released during the pyrolysis relative to the TOC (S2/TOC) in mg of HC per g of TOC. The HI is correlated to the H/C atomic ratio, which is used to determine the origin of the organic matter. Tmax is defined as the pyrolysis temperature at which the maximum amount of hydrocarbons is yielded by kerogen. Tmax increases linearly with the natural maturation degree of the organic matter, thus giving a rapid estimate of the thermal maturity of sedimentary basin rocks.

Raw data and percentages of some calcareous nannofossil species or group of species considered in this work were reported in Appendix A.

4. Results

4.1. Description of the Notre-Dame-de-Rosans section

A synthetic description of the Notre-Dame-de-Rosans section was first made by Friès (1987), and a more detailed sedimentological description is given by the same author in Friès and Parize (2003). This section (Fig. 2) starts with carbonate-dominated marlstone-limestone alternations (4 m) which represent the upper part of the Bedoulian limestones (Ferry, in Ferry and Rubino, 1989), and sharply end up by

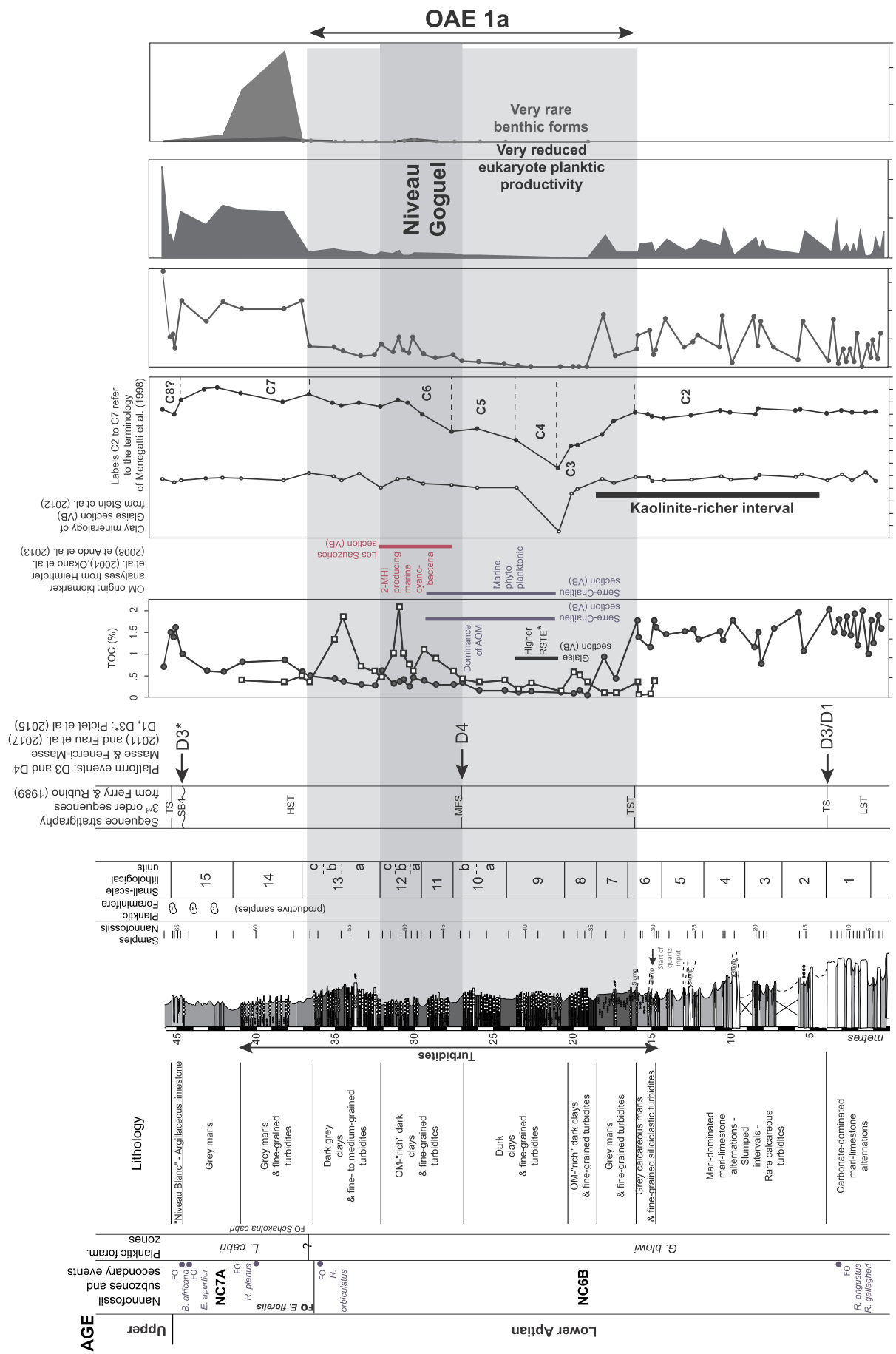

Fig. 2. Stratigraphic log, sample position, small-scale lithological units, calcium carbonate content, TOC, carbon and oxygen isotope data, calcareous nannofossil total absolute abundance and flux, and both planktic and benthic foraminifera absolute abundances from the Notre-Dame-de-Rosans section. Additional data from the literature are reported.

disappearance of limestone beds. Above the Bedoulian limestones, starts the Aptian-Albian Marnes Bleues Formation. This formation starts with the Bedoulian marl-dominated marlstone-limestone alternations disrupted by several submarine gravity-driven deposits (slumps, debrites and turbidites), derived from the western shelfbreak area (Ferry and Rubino, 1989). In the Early Aptian, turbidites are of calcarenitic origin (around 10-metre-thick; Fig. 2) and related to the rapid progradation (and thus the instability) of the Urgonian carbonate platforms (Ferry, in Ferry and Rubino, 1989). Slump set (Fig. 2) corresponds to the α slump of Friès (1987). These alternations are capped by one-metre-thick grey calcareous marlstones interrupted by fine-grained siliciclastic turbidites and slumps (Fig. 2). At the end of the Early Aptian, calcarenitic turbidites are replaced by sandy siliciclastic turbidites and correspond to the drowning of the Urgonian platforms and the development of a marly sedimentation (Bedoulian marlstones; Ferry, in Ferry and Rubino, 1989). An interval of two-metre-thick grey marlstones alternating with fine-grained siliciclastic turbidites and a last slump covered calcareous marlstones (Fig. 2). Marlstones are covered by a twenty-metre-thick interval of dark calcareous clays/clays alternating with fine-grained siliciclastic turbidites. These latter correspond to the P1 thin-bedded turbidite package described by Friès and Parize (2003). The clay interval starts with a first part of organic-matter rich dark clays, followed by dark clays, then a second part of organic-matter rich darks clays, and ends with dark grey clays (Fig. 2). The second organic-matter-rich part corresponds to the “Niveau Goguel”. The upper part of the succession is characterized by a ten-metre-thick grey marlstone interval which alternates in the five first metres with fine-grained siliciclastic turbidites (Fig. 2). The top of the succession is represented by a bundle of argillaceous limestones called the “Niveau blanc” which represents, as the “Niveau Goguel”, a lithological marker recognized in the whole Vocontian Basin (Friès, 1987; Bréhéret, 1997; Fig. 2).

Small-scale lithological units can be distinguished along the section (Fig. 2). A first unit is formed of 5 thick limestone beds separated by marlier alternations at its base and by marlstones (partly covered) at its top. Above, 5 small-scale lithological units are formed by marlstone-argillaceous limestone alternations where limestones are thin beds and commonly affected by superficial slumping (involving one or two beds). These units are separated from each other by thicker marly intervals. In the last unit (Unit 6 in Fig. 2) are recorded the first fine-grained siliciclastic turbidites. The next 8 small-scale lithological units are characteristically formed of packages of turbidites separated by decimetre- to metre-scale marlstones. Units 10, 12 and 13 (Fig. 3) can potentially be subidivided by thin marly intervals that separate small packages of turbidites. The last small-scale unit is formed of marlstones at its base and of argillaceous limestones at its top. In total, 15 small-scale lithological units are identified in the section, along with 20 small-scale units and sub-units (Fig. 2).

4.2. Calcareous nannofossil biostratigraphy

Nannofossil zones and subzones applied to the investigated section are the NC zones of Bralower et al. (1993, 1995) modified from Roth (1978; Fig. 2). This zonation scheme was selected because of its applicability to the low latitude Tethyan margin (Bralower et al., 1993). Biostratigraphic markers are illustrated in Fig. 3.

4.2.1. Chiastozygus litterarius Zone (NC6) of Early to “middle” Aptian age

The NC6 Zone was defined as the interval from the first occurrence (FO) of *Hayesites irregularis* to the FO of *Eprolithus floralis*. It was subdivided into the NC6A (lower) and NC6B (upper) subzones, defined by the FO of *H. irregularis* to the last occurrence (LO) of *Conusphaera rothii* and by the LO of *C. rothii* to the FO of *E. floralis*, respectively.

4.2.2. Subzone NC6B

Hayesites irregularis is already present in the first samples of the succession, as other species such as *Assipetra infracretacea larsonii* (large specimens of *Assipetra*), *Flabellites oblongus*, *Rhagodiscus angustus*, *Nannoconus truittii truittii* which are common in the Early Aptian; no specimens of *C. rothii* are observed at Notre-Dame-de-Rosans, suggesting that only the NC6B Subzone has been recognized. Bralower et al. (1993) observed that the LO of *C. rothii* is often difficult to identify in onshore sections due to both generally moderate preservation, and rarity of this taxon. *Nannoconus steinmannii* is not observed at Notre-Dame-de-Rosans. Its last occurrence is recorded within the NC6B Subzone (Bown et al., 1998). Erba et al. (1999) found that this species was rare in the Cismon core (southern Alps, Italy) and that determination of its LO is difficult to establish.

4.2.3. Rhagodiscus angustus Zone (NC7) of Late Aptian age

The NC7 Zone was defined as the interval from the FO of *E. floralis* to the FO of *Prediscosphaera columnata*. The NC7 Zone was subdivided into three subzones, called respectively A, B, and C.

4.2.4. Subzone NC7A

The NC7A Subzone was defined by the FO of *E. floralis* to the LO of *Micrantolithus hoschulzii*. This latter species is rare all along the succession, but is observed at the top, in the sample ROS66, and consequently the LO of this species is not observed in the Notre-Dame-de-Rosans section. This is in agreement with Herrle and Mutterlose (2003) who recognized the LO of *M. hoschulzii* above the “Niveau Noir” 4 (several metres above the “Niveau Blanc”) in the Serre Chaitieu section (Vocontian Basin). Both in the Cismon core (southern Alps, Italy; Erba et al., 1999) and in core drillings of Roquefort-la-Bédoule (South Provençal Basin, southeast France; Moullade et al., 2015), this species was very rare, and its LO difficult to determine. Moullade et al. (2015) questioned its application as a marker species.

In addition to the calcareous nannofossil zones, several nannofossil bioevents were recognized in the Notre-Dame-de-Rosans section allowing an accurate biostratigraphic framework to be established (Fig. 2). They are:

1. FOs of *Rhagodiscus angustus* and *R. gallagheri*
2. The “nannoconid crisis” (just above the dominant limestone-marlstone alternations)
3. FO of *Radiolithus orbiculatus* (4 m above black shales of the “Niveau Goguel”, sample ROS57)
4. FO of *Eprolithus floralis* (4.5 m above black shales of the “Niveau Goguel”, sample ROS58)
5. FO of *R. planus* and nannoconid return (8 m above black shales of the “Niveau Goguel”, sample ROS60)
6. FO of *E. apertior* (12.5 m above black shales of the “Niveau Goguel”, < 0.5 m below the “Niveau blanc”, sample ROS63)
7. FO of *Braarudosphaera africana* (13 m above black shales of the “Niveau Goguel”, within the “Niveau blanc”, sample ROS65).

4.3. Calcareous nannofossil assemblages

One sample (ROS 35) is barren of nannofossils (Appendix A). Calcareous nannofossil preservation is poor to good. Four classes of preservation are recognized (Appendix A). Class 1 (E3-O2) characterizes strongly etched and moderately overgrown specimens and is recognized in five samples (ROS6 and ROS 36-ROS 40); in these samples only few very poorly-preserved coccoliths are recognized. Class 2 (E2-O3) defines moderately etched and strongly overgrown specimens; samples showing this preservation category do not present low species richness. Class 3 (E2-O2) characterizes moderately etched and overgrown specimens and is recognized in most samples. Class 4 (E1-O1) characterizes both slight etched and overgrown specimens and corresponds to good preservation. A total of 102 species is recorded. The total absolute abundance shows significant variations, with an average of 8.5×10^8 nannofossils/g of rock. It sharply decreases in Unit 8 until the “Niveau Goguel” (26 m), with values comprised between 0 and

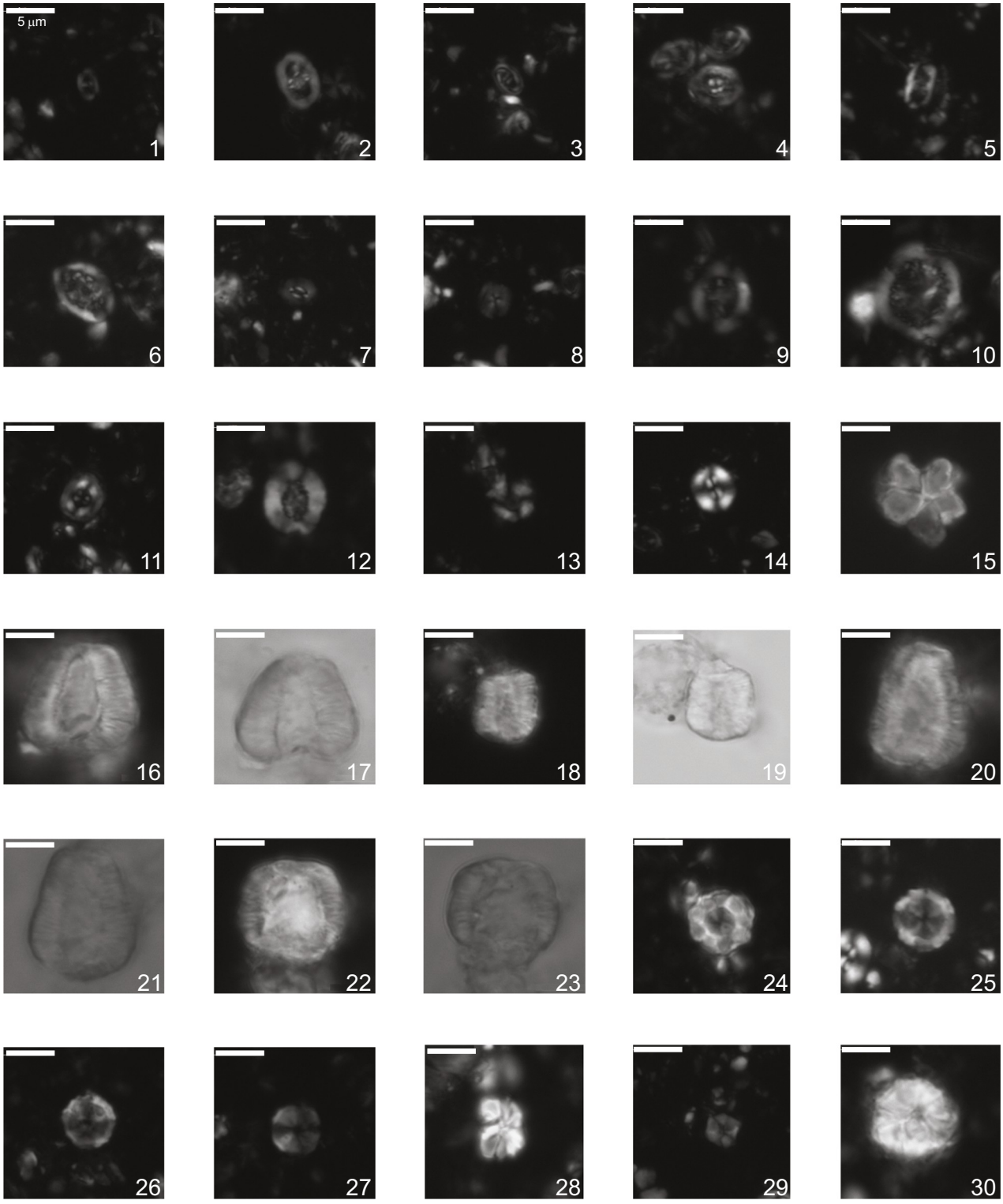

Fig. 3. Photomicrographs of selected nannofossil species from the Notre-Dame-de-Rosans section. 1, *Zeugrhabdotus erectus*, XLP, sample Ros66. 2, *Zeugrhabdotus scutula*, XLP, sample Ros68. 3, *Zeugrhabdotus xenotus*, XLP, sample Ros67. 4, *Rhagodiscus achlyostaurion*, XLP, sample Ros67. 5, *Rhagodiscus angustus*, XLP, sample Ros67. 6, *Rhagodiscus asper*, XLP, sample Ros68. 7, *Biscutum ellipticum*, XLP, sample Ros68. 8, *Discorhabdus rotatorius*, XLP, sample Ros68. 9, *Cretarhabdus conicus*, XLP, sample Ros68. 10, *Retecapsa surirella*, XLP, sample Ros68. 11, *Flabellites oblongus*, XLP, sample Ros68. 12, *Retecapsa crenulata*, XLP, sample Ros66. 13, *Diazomatolithus lehmannii*, XLP, sample Ros65. 14, *Watznaueria barnesiae*, XLP, sample Ros63. 15, *Braarudosphaera africana*, XLP, sample Ros65. 16–17, *Nannoconus bucheri*, XLP (16) and TL (17), sample Ros64. 18–19, *Nannoconus truittii truittii*, XLP (18) and TL (19), sample Ros65. 20–21, *Nannoconus vocontiensis*, XLP (20) and TL (21), sample Ros65. 22–23, *Nannoconus wassallii*, XLP (22) and TL (23), sample Ros65. 24, *Eprolithus floralis*, XLP, sample Ros68. 25, *Radiolithus orbiculatus*, XLP, sample Ros68. 26, *Radiolithus planus*, XLP, sample Ros68. 27, *Radiolithus varolii*, XLP, sample Ros68. 28, *Assipetra infracretacea*, XLP, sample Ros63. 29, *Hayesites irregularis*, XLP, sample Ros66. 30, *Rucinolithus terebrodentarius*, XLP, sample Ros63.

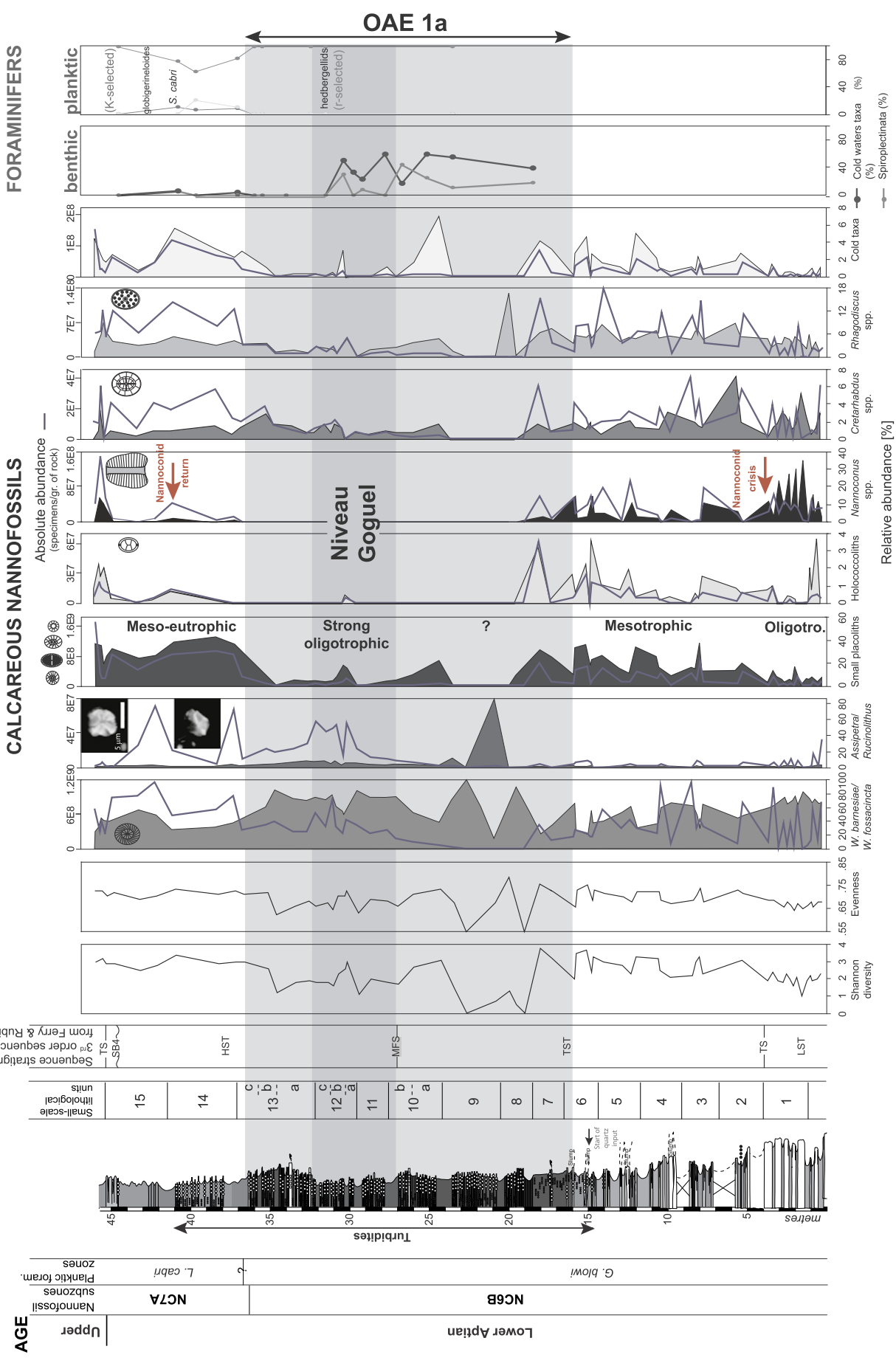

Fig. 4. Vertical distribution of calcareous nannofossil diversity and evenness, both absolute and relative abundances of selected nannofossil taxa and relative abundances of selected planktic and benthic foraminifera taxa from the Notre-Dame-de-Rosans section.

2.14×10^8 nannofossils/g of rock, and increases from the "Niveau Goguel" up to the top of the succession with maximal value of 3.42×10^9 nannofossils/g of rock (Fig. 2). A similar trend is observed for nannofossil fluxes, with lowest values recorded in the interval corresponding to Units 8 to 10b (values comprised between 0 and 1.9×10^{11} nannofossils/m^2/yr), and highest values in the upper part of the succession (Units 14–15; values comprised between 0.7 and 4.7×10^{11} nannofossils/m^2/yr; Fig. 2). Average Shannon Index and evenness values are 2.25 and 0.47, respectively, but these variables describing diversity of nannofossil assemblages strongly fluctuate with more or less the same trend as already recognized for both absolute abundance and flux (Fig. 4). Diversity increases in the lower part of the succession (Units 2 to 7; Shannon Index values are comprised first between 1 and 2, then between 2 and 4); poorly-diversified assemblages are recorded in Units 8 to 10a (Shannon index values below 1), and more diversified assemblages are observed in the upper part of the succession (Units 14–15; Shannon Index values are comprised between 1.5 and 3.5; Fig. 4). Nannofossil taxa or group of taxa presented in Fig. 4, are those which significantly contribute to the total assemblage and/or present large fluctuations both in absolute and relative abundances. They are also illustrated in Fig. 3. They present for their absolute abundance a general trend similar to the total nannofossil absolute abundance, which represent large fluctuations in the lower part of the succession, lowest values in Units 8 and 9, increasing values just below or within the "Niveau Goguel", and highest values in the upper part of the succession (Units 14–15; Fig. 4). Coccoliths significantly contributing to the nannofossil assemblage (around 80% in total with an average relative abundance higher than 1% for each group) are described in decreasing order of abundance as follows: *Watznaueria barnesiae/W. fossacincta*, the small placoliths group, *Rhagodiscus* spp., and *Cretarhabdus* spp. *Watznaueria barnesiae/W. fossacincta* lumped together because they represent end-members of a morphological continuum (Lees et al., 2004, 2006; Bornemann and Mutterlose, 2006). Average absolute and relative abundances of *W. barnesiae/W. fossacincta* is 3.9×10^8 nannofossils/g and 56.7%, respectively (Fig. 4). Relative abundance does not present the same trend as absolute abundance, and shows highest values in Units 9 to 13a (Fig. 4). The small placoliths include, in decreasing order of abundance, dominant *Discorhabdus rotatorius*, *Biscutum ellipticum* (considered as a morphotype of *B. constans* by Bornemann and Mutterlose, 2006), small *Zeugrhabdotus* (*Z. erectus* + *Zeugrhabdotus* with major axis smaller than 5 μm), and very rare *Diazomatolihtus lehmanii*. They were grouped since they have been interpreted by many authors as eutrophic or meso-eutrophic taxa (Roth, 1981; Roth and Bowdler, 1981; Roth and Krumbach, 1986; Erba, 1987, 1992; Crux, 1989; Premoli Silva et al., 1989; Roth, 1989; Watkins, 1989; Coccioni et al., 1992; Erba et al., 1992; Williams and Bralower, 1995; Mutterlose and Kessels, 2000; Street and Bown, 2000; Bersezio et al., 2002; Giraud et al., 2003; Erba and Tremolada, 2004; Linnert et al., 2010; Mattioli et al., 2014). Both absolute and relative abundances of this group show the same trend with low values in Units 1, 8 to 13a, moderate values in Units 2 to 7, and high values in Units 14–15 (Fig. 4). Average absolute abundance is 1.9×10^8 nannofossils/g (with averages of 8.5×10^7 nannofossils/g, 5.7×10^7 nannofossils/g, and 5.2×10^7 nannofossils/g, respectively for the different species or group of species). They are common (average value of 15.3%), with means of 7.1%, 4.3%, and 3.9%, respectively (Fig. 4). *Rhagodiscus asper* (which are dominant) and *R. achlyostaurion* are grouped (*Rhagodiscus* spp.) since they are considered as indicative of low-latitude warm sea-surfaces (Roth and Krumbach, 1986; Erba, 1987, 1992; Crux, 1989, 1991; Premoli Silva et al., 1989; Erba et al., 1992; Bralower et al., 1993; Williams and Bralower, 1995; Mutterlose and Kessels, 2000). This group presents an average absolute abundance of 3.4×10^7 nannofossils/g. It is common with an average relative abundance of 4.1%, and shows higher percentages in the lower part of the succession from Units 1 to 8, with respect to the rest of the succession (Fig. 4). *Cretarhabdus* spp. (including all species of the genera *Cretarhabdus* and *Retecapsa*; Roth and Krumbach, 1986) present more or less the same trend for absolute abundances than those of *Rhagodiscus* spp.; their mean absolute abundance equals to 1.1×10^7 nannofossils/g; they are frequent with mean of 1.5%, but decrease in percentages from Units 3 to 7, and become very rare or absent in Units 8 and 9 (Fig. 4). The group *Assipetra/Rucinolithus*, including dominant *A. infracretacea* and few *R. terebrodentarius*, is presented because it shows a very large peak of relative abundance around 21 m (Unit 9; Fig. 4); its absolute abundance (mean of 1.1×10^7 nannofossils/g) increases in the upper part of the succession from the "Niveau Goguel" (Units 11 to 15; Fig. 4). Large-sized specimens of both species are recognized in the Notre-Dame-de-Rosans section, but are few and do not increase in abundance during the Early Aptian as it was recognized for other sections (Serre Chaitieu: Vocontian Basin, Herrle and Mutterlose, 2003; Cismon core: northern Italy, Tremolada and Erba, 2002, Erba and Tremolada, 2004; DSDP Site 463: Pacific, Tremolada and Erba, 2002, Erba and Tremolada, 2004). Holococcoliths are notably present in the lower part of the succession (Units 1 to 7), and show means of 1.2×10^7 nannofossils/g and 1%, respectively in this interval (Fig. 4). Absolute abundance of *Nannoconus* spp. (average of 3.1×10^7 nannofossils/g) is maximum at the top of the section (Unit 15) and *Nannoconus* spp. are also well present in the lower part of the succession (Units 2 to 7; Fig. 4), but they are even common to abundant in the lowest part of the succession where they can reach up to 35% (Unit 1; Fig. 4) whereas they are very scarce or absent in Units 8 to 13a; they present a mean value of 4.6% for the whole succession. The following species, *Repagulum parvidentatum* (which is dominant), *Rhagodiscus angustus*, *Seribiscutum gaultensis* and *Sollasites horticus* are grouped because their distribution are primarily controlled by temperature (Wise, 1988; Erba et al., 1989; Crux, 1991; Mutterlose, 1992; Watkins et al., 1996; Mutterlose and Kessels, 2000; Street and Bown, 2000; Melinte and Mutterlose, 2001). Both absolute and relative abundances of this cold-water assemblage, are presented with averages of 1.8×10^7 nannofossils/g and 1.5%, respectively (Fig. 4). Their highest absolute abundances are recorded at the top of the succession. They show both low absolute and relative abudances in the lowermost part of the succession (Unit 1). Higher percentages are recorded in Units 4 to 7 and 14 to 15 with respect to the rest of the succession and the maximum value (7.1%) is observed in Unit 10a (Fig. 4).

4.4. Foraminifera

Foraminifers are overally not abundant (Fig. 2). Planktics are poorly diversified and represented by only 8 taxa. Benthics comprised 46 taxa. Four assemblages were defined (Fig. 5).

The first two assemblages correspond to Units 8 to 13 in which foraminifers are scarce or absent. Their number per gram of sediment is very low, with a maximum at the base of Unit 12 (35 specimens; Fig. 2).

In the first assemblage (Units 8 to 12b), planktic foraminifers are usually absent (even in the < 63 μm fraction) or very scarce and then represented by only one species (*Hedbergella sigali*). Benthic foraminifers comprised mostly Textulariina (45 to 100%) represented by Verneuilinidae (*Spiroplectinata robusta*, *Gaudryinella sherlocki*, *Glomospirella gaultina*, *Tritaxia tricarinata*), Haplophragmiidae (*Haplophragmoides* sp.), Ammmodiscidae (*Ammodiscus cretaceous*), Lituolidae (*Ammobaculites* sp.), Hormosinidae (*Reophax* sp.), Spirillinidae (*Spirinilla minima*), Eggerelllidae (*Choffatella decipiens*), Textuariidae (*Textularia minuta*). Lagenina are less abundant (5 to 30%) except in the "Niveau Goguel" in which they reach 40%. They comprise mostly Vaginulinidae (*Lenticulina nodosa*, *Astacolus crepidelaris*, *Vaginulina truncata*, *Cytharinella* sp.), with scarce Nodosariidae (*Dentalina*) and Lagenidae (*Lagena*) in a few samples. Rotaliina are lacking or scarce, except in Unit 12 in which they reach 35%. They comprise mostly Gavelinellidae (*Gavelinella* sp.), with sometimes some Buliminidae (*Uvigerina*), Pleurostomellidae (*Pleurostomella* sp.) or Globorotalitidae (*Globorotalites aptiensis*). In Unit 9, *Globorotalites*

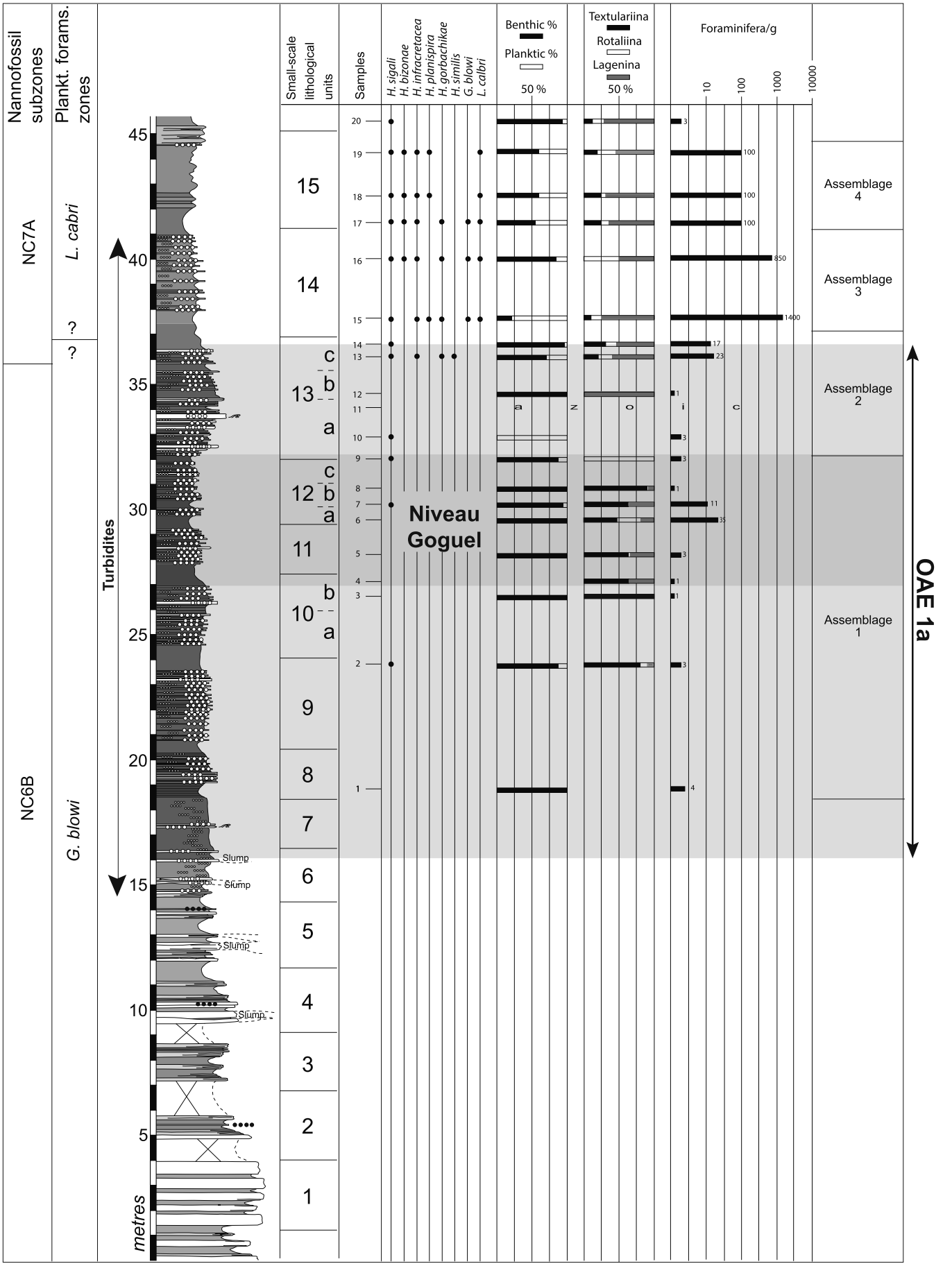

(caption on next page)

Fig. 5. Distribution of planktic foraminifera. Percentages of planktic and benthic foraminifera, percentages of Textularina, Rotalina and Lagenina, number of foraminifera per gram of sediment.

aptiensis is the only species present. This first assemblage is thus characterized by a poor foraminiferal fauna, with very scarce planktics, and benthic populations mostly represented by agglutinated like Verneuilinids, Eggerellids, Ataxophragmiids, Hormosinids, and uncoiled Lituolids. Benthic associations belong to morphogroup AG.A of Koutsouskos and Hart (1990).

The second assemblage is restricted to Unit 13. Foraminifers are still poorly abundant, with a maximum of twenty specimens per gram of sediment. Within Unit 13a, they are either absent or scarce. Planktics comprises *Hedbergella sigali*, *H. infracretacea*, *H. gorbachikae* and *H. similis*. They are scarce or absent. The main change versus the first assemblage concerns benthics which are now dominated by calcareous forms, especially by Lagenina (50 to 75%), associated to Textulariina (about 25%) and Rotaliina (< 10%). Lagenina comprises Vaginulidae (*Lenticulina nodosa*, *L. rotulata*, *L. ouachensis*, *Marginulina variata*, *Astacolus crepidularis*), Nodosaridae (*Nodosaria sceptum*, *N. pauperculae*, *Frondicularia* sp., *Dentalina* sp.), and Polymorphinidae (*Ramulina*). Textulariina are less abundant and less diversified than in assemblage 1. They comprise Verneuillinidae (*Dorothia levis*, *Tritaxia pyramidata*, *Gaudryina* sp.) and Eggerellidae (*Choffatella*. sp., *Dorothia levis*). Rotaliina are represented by Gavelinellidae (*Gavelinella* gr. *flandrini*), Pleurostomellidae (*Pleurostomella obtusa*) and Bagginidae (*Valvulineria* sp.). Compared to the first assemblage, this second assemblage remains poor in foraminifers, especially planktics. Its main characteristic is the change occurring within benthics with the high percentage of Lagenina dominated by Vaginulinidae with coiled morphotypes. This benthic association belong to morphogroup CH-B3 of Koutsouskos and Hart (1990).

The third assemblage (Unit 14) is characterized by abundant foraminifers (up to 1400 specimens per gram of sediment). Planktics are dominant (80%). Planktic foraminifers are represented by 7 taxa (*H. sigali*, *H. bizonae*, *H. infracretacea*, *H. planispira*, *H. gorbachikae*, *G. blowi* and *L. cabri*). Benthic foraminifers are again dominated by Lagenina (50 to 75%) associated with Texulariina (10 to 25%) and Rotaliina (10 to 25%). Lagenina are well-diversified and dominated by Vaginulidae (*Marginulina variata*, *Lenticulina rotulata*, *L. nodosa*, *N. obscura*, *Planularia complanata*, *Astacolus evoluta*, *A. gaultina*, *Vaginulina* sp., *Vaginulinopsis* sp.). To Lagenids are associated Nodosariidae (*Dentalina variata*, *Dentalina, inconstans*) and Lagenidae (*Lagena* sp.). Textulariidae comprises Haplophragmiidae (*Haplophragmoides* sp.), Ataxophragmiidae (*Arenobulimina* sp.), Eggerelidae (*Dorothia levis*, *Choffatella decipiens*), Verneuilinidae (*Tritaxia pyramidata*) Lituolidae (*Ammobaculites* sp.), Ammodiscidae (*Ammodiscus cretaceus*). Rotaliina are represented by Gavelinellidae (*Gavelinella* gr. *flandrini*), Golorotalitidae (*Globorotalites* sp.) and Pleurostomellidae (*Pleurostomella* sp.). This third assemblage is thus characterized by the abundance and the diversity of planktic foraminifers as well as for benthics. Calcareous benthics are prominent with always the dominance of Lagenina, and especially Vaginulinidae with coiled morphotypes, that is still morphogroup CH·B3 of Koutsouskos and Hart (1990).

The fourth assemblage develops in Unit 15. Foraminifers are still abundant (100 specimens per gram of sediment), except in the last sample. Planktic associations are similar to those of assemblage 3. *L. cabri* is still well represented. Benthic foraminifers are dominated by Lagenina (50 to 75%) associated to Textulariina (25%) and Rotaliina (< 10% to 25%). So, associations do not differ from assemblage 3, except for the proportions between planktics and benthics. Except for the last sample (above the "Niveau blanc"), benthic foraminifers become indeed more abundant (60%) than planktics. They belong always to morphogroup CH3-B3 of Koutsouskos and Hart (1990).

The first two assemblages belong to the *G. blowi* Interval Zone. The first occurrence of *L. cabri* (species characterizing the Acme Zone of the nominal taxon) is at base of Unit 14. The use of the first occurrence of *L. cabri* to characterize the base of the zone is difficult because this species is at first scarce. The first occurrence of *L. cabri* (species characterizing the Acme Zone of the nominal taxon) lies at base of Unit 14. The use of the first occurrence of *L. cabri* to characterize the base of the zone is difficult because this species is at first scarce. Generally, in the Tethys, it becomes more abundant later (Premoli Silva et al., 1999) and its first occurrence coincides with the end of the OAE 1a (Luciani et al., 2006). So, the base of the *L. cabri* Zone is placed accordingly in the section studied here.

4.5. Calcimetry and carbon and oxygen stable isotopes

The range of the calcium carbonate content varies from 1.6 to 89.6% (Fig. 2); it sharply decreases at 16 m, with very low values in Units 8 to 10b. It increases from the "Niveau Goguel" up to the top of the succession (Fig. 2).

The stable carbon isotope values vary between −2.3 and +4.1‰ (Fig. 2). From Units 1 to 6, they are generally constant around 2‰ (Fig. 2). Then, a large decrease of 4‰ is recognized with a minimum value at 20.5 m (Unit 9; Fig. 2). This is followed by a large increase of 5.5‰ up to Unit 12a, where a value of 3.1‰ is recorded (Fig. 2). The higher part of the succession is characterized by gently increasing values up to 4.1‰ at 40.5 m (unit 4; Fig. 2). After that, a decrease of > 2‰ is observed up the "Niveau blanc" (Fig. 2). The carbon isotope data acquired at Notre-Dame-de-Rosans allow the different chemostratigraphic segments, from C2 to C8, to be recognized as defined by Menegatti et al. (1998; Fig. 2).

The stable oxygen isotope values vary between −7.4 and −2.7‰ and follow the same trend with respect to the stable carbon isotope record, but with lower magnitude fluctuations (around 1‰) from 23 m to the top of the succession (Fig. 2).

4.6. Rock Eval

The 32 studied samples contain between 0.09 and 2.06% TOC, and there is no clear relationship between TOC % and $CaCO_3$% (Fig. 2). Half of the samples displays organic matter contents lower than 0.4%. Such low values are in the range of normal marine shales deposited in oxygenated waters. Only the samples around the bed ROS-50 show TOC contents between 1% and 2%. Such values were usually recorded in lower Aptian black shales of the Vocontian Basin although the "Niveau Goguel" may show a higher organic content in some sections (up to 5%; Bréhéret, 1997). Temperatures of maximum pyrolytic yield (Tmax) are in the range of 421 °C to 432 °C for samples having an organic richness higher than 0.25%.

5. Interpretations

5.1. Sequence- and cyclostratigraphy

Different sequence stratigraphic interpretations for the Upper Barremian-Aptian have been presented by Ferry, in Ferry and Rubino (1989) as well as Friès and Parize (2003) at the basin scale. Friès and Parize (2003) used the following criteria for their sequence stratigraphic interpretation (sensu Posamentier and Vail, 1988): 1) The large-scale regional erosional surfaces define sequences boundaries; 2) units formed of limestone bundles correspond to lowstand prograding wedge in which common gravity deposits (slumps, debrites and turbidites) are recorded; and 3) the condensed intervals and the overlying black shales which extend onto the shelf represent maximum flooding surfaces. The recognition of a large-scale discontinuity in the Notre-

Table 1
Dissolution susceptibility of selected calcareous nannofossil taxa encountered in this study. *Biscutum ellipticum* is considered as a morphotype of *B. constans* (Bornemann and Mutterlose, 2006).

Taxa	Susceptibility to dissolution
Biscutum constans/B. ellipticum	Dissolution-susceptible[a,b,c,d,e,f]
Discorhabdus rotatorius	Dissolution-susceptible[g]
Zeugrhabdotus erectus	Dissolution-susceptible[a,d,g]
Small *Zeugrhabdotus* (with major axis ≤ 5 μm)	Dissolution-susceptible[a,f]
Watznaueria barnesiae	Dissolution-resistant[a,b,c,d,e,f,g,h]
Holococcoliths	Dissolution-susceptible[b,i,j,k]

[a] Hill (1975).
[b] Thierstein (1980).
[c] Roth and Bowdler (1981).
[d] Roth and Krumbach (1986).
[e] Roth (1981).
[f] Mutterlose and Wise (1990).
[g] Thierstein and Roth (1991).
[h] Bornemann and Mutterlose (2006).
[i] Okada and McIntyre (1977).
[j] Schneidermann (1977).
[k] Tappan (1980).

Dame-de-Rosans section few metres below the beginning of the presented-here logged section led Friès and Parize (2003) to interpret the base of the section as lowstand deposits as being formed by limestone bundles. The occurrence of slumps and turbidites from 5 to 41 m in Fig. 2 led these authors to consider this interval as well as the above lying "Niveau Blanc" as belonging to the same lowstand system tracts. The marly interval on top of the section is then interpreted as being deposition during transgression. In this interpretation, the black shales of the "Niveau Goguel" are not regarded as maximum flooding deposits, even black shale deposition is one of the criteria used by the authors to define maximum flooding surfaces. The absence of a condensed interval below the black shales possibly explains this apparent contradiction. However, the frequent input of siliciclastic turbidites in the Notre-Dame-de-Rosans section may have prevented the formation of a condensed interval.

Ferry, in Ferry and Rubino (1989) by comparing and correlating the stratigraphic relationship between the shallow-water carbonate series of the Ardèche area (eastern flank of the "Massif Central") and the Vocontian Basin proposed that the limestone-dominated intervals in the basin correspond to the progradation during falling sea-level of platform environments testified by the recognition along the slope of several hundred metres-wide channels filled by bioclastic platform material. These authors proposed that the backstepping of platform carbonate banks during transgression well explains the reduction of carbonate export to the basin, and then interpreted the changes from carbonate-dominated to marl-dominated as corresponding to transgressive intervals. In these transgressive deposits, slump deposits are recognized. Ferry and Rubino (1989) interpreted the organic-rich intervals such as the "Niveau Goguel" as corresponding to the maximum flooding as it is commonly observed in other basins and for other time intervals (e.g., Razin et al., 2017). Thus, the most carbonate-rich intervals in the Notre-Dame-de-Rosans section are interpreted as lowstand deposits (from 0 to 4 m in the studied sections, and the "Niveau Blanc"), the interval from 4 m to the base of the "Niveau Goguel" as the transgressive deposits, and the interval above the "Niveau Goguel" as highstand deposits.

On the long term (2nd-order sequences sensu Vail et al., 1991), the sequence stratigraphic interpretation of Ferry and Rubino (1989) and Friès and Parize (2003) does not differ, but Ferry and Rubino (1989) provided shorter-term (3rd order) information on sea-level fluctuations. The sequence stratigraphic interpretation (sensu Posamentier and Vail, 1988) of Ferry, in Ferry and Rubino (1989) for the Notre-Dame-de-Rosans section is in agreement with interpretations performed in carbonate plaform environments in e.g. Oman (Pittet et al., 2002), Italy (D'Argenio et al., 2004) or Spain (Bover-Arnal et al., 2009), and is here preferred because providing more details for the studied interval than that of Friès and Parize (2003).

The small-scale lithological units identified in the section (Fig. 2) possibly translate short-term environmental changes. Given the duration of the OAE 1a of 1.15 to 1.4 Myr estimated by cyclostratigraphy (Li et al., 2008; Huang et al., 2010; Malinverno et al., 2010; Lorenzen et al., 2013; Moullade et al., 2015), the small-scale units (7 to 13) would have an average duration of 164 to 200 kyr. Taking into account the small-scale units plus sub-units (Fig. 2), their average duration is 96 to 116.7 kyr, which is close to the duration of the short eccentricity (Berger et al., 2005). We therefore interpret the origin of these small lithological units and subunits as resulting from an eccentricity forcing on sedimentation. Units 1 to 5 are generally formed of packages of 3 to 5 marlstone-limestone alternations, possibly translating a precession-eccentricity hierarchy, even poor outcropping conditions and superficial slumping in Units 2 to 5 does not allow to precisely constrain this hierarchical organization of cycles. Unit 6 is a transitional small-scale unit that starts with marlstone-limestone alternations but records higher the first input of siliciclastic turbidites that characterize the OAE 1a (Fig. 2). It is therefore difficult to attribute an origin to its formation. However, an eccentricity control on the formation of most of the units and sub-units is likely (even not definitely proven), and allows for an estimation of the duration of the different phases of environmental conditions before, during and after the OAE 1a.

5.2. Calcareous nannofossils preservation at Notre-Dame-de-Rosans

Preservation of nannofossils depends on lithology and is generally lower in limestones than in marlstones due to increasing diagenesis in limestones (Roth and Thierstein, 1972). In the Notre-Dame-de-Rosans section, the calcium carbonate content is highly variable and its effect on the nannofossil preservation state was tested. Thierstein and Roth (1991) shown that best-preserved specimens are observed in samples with calcium carbonate contents comprised between 40 and 60%. We have tested the recognized effects of calcium carbonate content on nannofossil total abundance, species richness, relative abundance of delicate small placoliths (*Biscutum ellipticum* + *Discorhabdus rotatorius* + small *Zeugrhabdotus*; Table 1), and relative abundance of holococcoliths, which are generally rare in the fossil record, due to their low preservation potential (Table 1). Herrle (2002) observed increased relative abundance of holococcoliths within the lower Albian "Niveau Paquier" black shale of the l'Arboudeysse section (Vocontian Basin), that he interpreted to be probably due to the higher amount of organic matter which may have increased the preservation potential of holococcoliths. Holococcoliths are present in some intervals of the Notre-Dame-de-Rosans section, but are rare or absent in the "Niveau Goguel". We have also added in these graphs the four classes of preservation recognized (Fig. 6). Low nannofossil total abundances are recorded both in samples with highest (> 78%) and lowest (< 25%) calcium carbonate contents, corresponding to different preservation states. Lowest nannofossil total abundances correspond to lowest calcium carbonate contents, and to very poorly-preserved (strong etching) specimens. There is no correlation between species richness and calcium carbonate content; only four very poorly-preserved samples with lowest species richness correspond to lowest calcium carbonate contents. There is no correlation between the relative abundance of delicate taxa and the calcium carbonate content; highest percentages of delicate taxa are recorded in samples with calcium carbonate contents higher than 20% and lower than 70% and with preservation state varying from poor to good. There is a positive correlation ($r = 0.491$, $p < 0.0001$) between the relative abundance of holococcoliths and the calcium carbonate content but it is not linked to the preservation state of holococcoliths. We conclude that at Notre-Dame-de-Rosans, preservation state of nannofossils weakly depends on lithology. The same

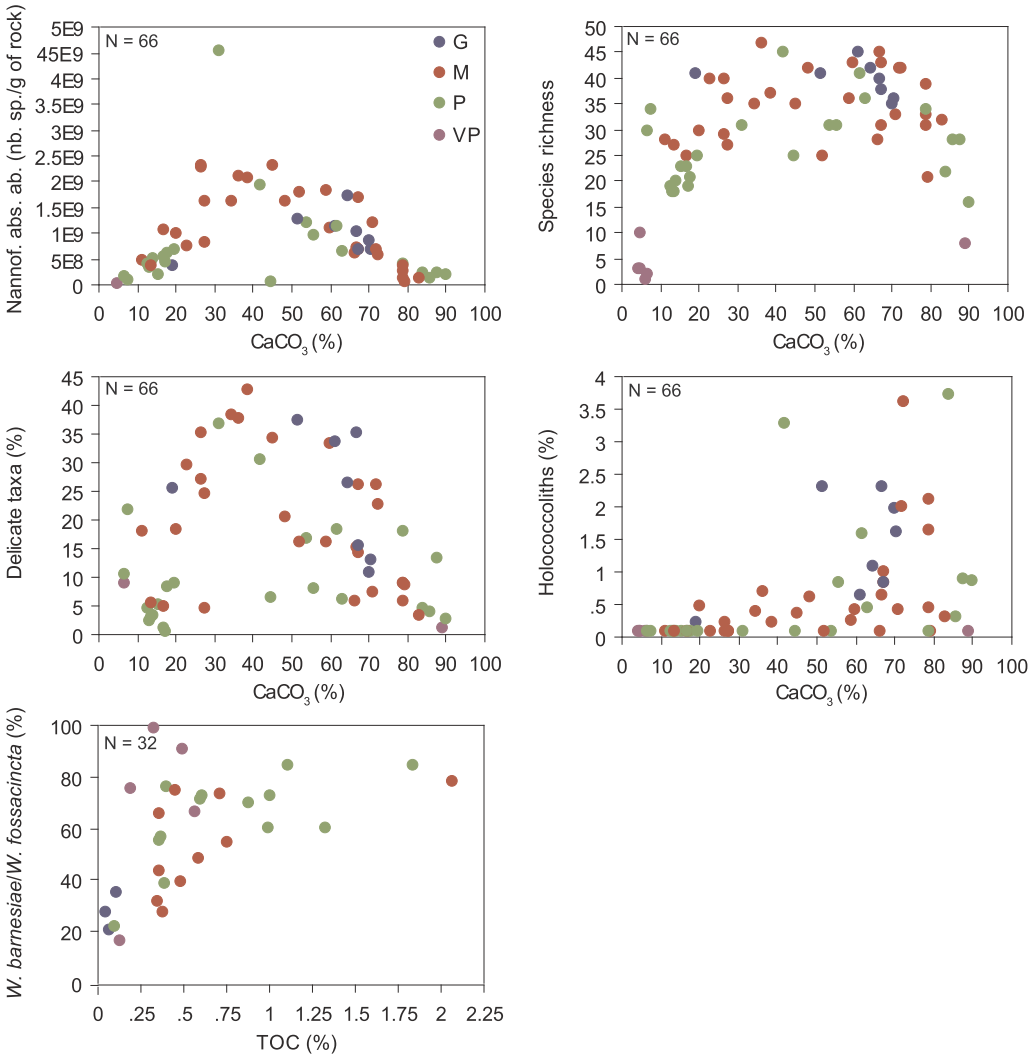

Fig. 6. Bivariate plots showing the relationship between 1) $CaCO_3$ content and calcareous nannofossil abosulte abundance, 2) $CaCO_3$ content and species richness, 3) $CaCO_3$ content and relative abundance of nannofossil delicate taxa, 4) $CaCO_3$ content and relative abudance of holococcoliths, and 5) TOC content and relative abundance of *W. barnesiae/W.fossacincta* for different classes of preservation, recognized in the Notre-Dame-de-Rosans section. Abbreviations: N, number of measurements; G, good preservation; M, moderate preservation; P, poor preservation; VP, very poor preservation.

conclusion was derived by Erba (1994), Erba and Tremolada (2004), Erba and Tremolada (2004) and Erba et al. (2010).

Impoverished nannofossil assemblages (strongly etched) recorded in samples ROS36 to ROS40 (Units 8–9, upper part of carbon isotope segment C3 to C4; Fig. 2) are indicative of carbonate dissolution. Highest values of both *Watznaueria barnesiae/W. fossacincta* and *Assipetra/Rucinolithus* percentages are recorded in this interval. Among the *Watznaueria* group, characterized by thick placoliths with strongly imbricated elements, and considered to be more resistant to dissolution than other coeval nannofossils, due to their robust morphology (Roth and Bowdler, 1981), *W. barnesiae*, with its closed central area, is considered to be one of the more resistant to dissolution (Table 1). *Assipetra infracretacea* and *R. terebrodentarius* are very robust calcified nannoliths which could also be fairly resistant to dissolution, as suggested by Bergen (1998). High organic carbon in sediments can be responsible for etching of coccoliths (Roth and Krumbach, 1986). Decay of organic matter by bacteria increases dissolved carbon dioxide content of pore waters and results in carbonate dissolution (Roth and Krumbach, 1986). Using the *Watznaueria* group, Roth and Krumbach (1986) showed that a positive correlation between the relative abundance of *Watznaueria* spp. and the organic carbon content of sediments is a measure of carbonate dissolution. We have then tested the correlation between the relative abundance of *W. barnesiae/W. fossacincta* (Table 1) and the TOC in the Notre-Dame-de-Rosans section (Fig. 6). Despite the fact that a positive correlation ($r = 0.522$, $p < 0.0022$) is observed, high percentages of *W. barnesiae/fossacincta* observed in impoverished assemblages do not correspond to high total organic content. Impoverished assemblages correspond to samples with lowest calcium carbonate contents (< 8%, Fig. 2). Critical decrease in the calcium carbonate content observed in this interval does not result from oxidation of organic matter and early diagenesis. This decrease could result from: 1) high dissolution due to early diagenetic processes within the pore waters, 2) a high dissolution rate at the sediment-water interface induced by a shallowing of the calcite lysocline/CCD, which was invoked for other settings by Erba (1994), Erba and Tremolada (2004), Erba and Tremolada (2004), Erba et al. (2010). We will further discuss these two hypotheses.

5.3. Time succession in calcareous nannofossil asssemblages at Notre-Dame-de-Rosans

In the lowermost part of the succession (Unit 1, lowermost part of the carbon isotope segment C2), nannofossil primary productivity was low, as suggested by both low nannofossil fluxes and abundances of small placoliths (Fig. 4). Low trophic levels could explain high

abundances of *W. barnesiae/W. fossacincta* (Fig. 4), which has been associated with oligotrophic conditions by many authors (Roth, 1986, 1989; Roth and Krumbach, 1986; Erba et al., 1992; Williams and Bralower, 1995; Herrle, 2003). However, as seen in Section 4.3, both absolute and relative abundances of this group do not present the same trends. In particular, in Unit 1, *W. barnesiae/W. fossacincta* presents large fluctuations in its absolute abundance but weak fluctuations in its relative abundance (Fig. 4). Moreover, within the OAE 1a interval, whereas the absolute abundance of this group is low, as for all the nannofossil assemblages, its percentage presents the highest values. All these observations show that *W. barnesiae/W. fossacincta* is eurytopic, able to adapt to fluctuating environmental conditions, as already suggested by different authors (Mutterlose, 1991; Mutterlose and Kessels, 2000; Street and Bown, 2000; Aguado et al., 2014). The same conclusion was derived by Giraud et al. (2003) from the study of calcareous nannofossil assemblages across the latest Albian "Niveau Breistroffer" (OAE 1d) in the Vocontian Basin. Low trophic levels prevailing within Unit 1 can also be inferred from the relative abundances record of both *Nannoconus* spp. and holococcoliths, which present for the former highest percentages in this unit, and for the latter, a peak recorded at the base (Fig. 4). More general, *Nannoconus* spp. and holococcoliths show similar trends throughout the succession (Fig. 4), possibly due to similar ecological preferences. *Nannoconus* spp. are generally considered as low-latitude and rather epicontinental and warm-waters taxa (Roth, 1981; Roth and Bowdler, 1981; Roth and Krumbach, 1986; Mutterlose, 1989; Bralower et al., 1993; Scarparo Cunha and Shimabukuro, 1997; Mutterlose and Kessels, 2000; Street and Bown, 2000; Melinte and Mutterlose, 2001; Mutterlose et al., 2003; Lees et al., 2005). They have been interpreted by different authors as oligotrophic (Tappan, 1980; Busson and Noël, 1991; Coccioni et al., 1992; Erba, 1994; Mutterlose and Kessels, 2000), but mesotrophic conditions have also been suggested by others (Scarparo Cunha and Shimabukuro, 1997; Pauly et al., 2012). Erba (1994) first supposed that *Nannoconus* spp. were deep-dweller that flourished when the surface waters were oligotrophic and the nutricline was deep. Herrle (2003) and Bornemann et al. (2005) have studied among others the temporal abundance pattern of *Nannoconus* spp. in some sections of the Vocontian Basin across the Early Albian OAE 1b and the latest Albian OAE 1d, respectively. They both concluded that nannoconids flourished when, in a stratified water column, the upper photic zone was impoverished in nutrients and the nutricline was deep. Herrle (2002) observed in the "Niveau Paquier" that the occurrence of holoccoliths (*Orastrum* spp.) partly corresponds with that of *Nannoconus* spp. (Early Albian, l'Arboudeysse section). In modern oceans, holococcolithophores are surface-dwellers (Cros et al., 2000) and are most abundant in oligotrophic and stratified water masses (Kleijne, 1991; Brand, 1994; Winter et al., 1994). Renaud and Klaas (2001) have also shown that their occurrence was associated with the onset of water stratification and subsequent depletion in nutrients; this means they proliferate during transitional periods in terms of nutrient levels. For the fossil record, Perch-Nielsen (1985) interpreted the occurrence of holococcoliths as characteristic of shelf environments in epicontinental seas. At Notre-Dame-de-Rosans, the peak in the relative abundance of holococcoliths recorded at the base of Unit 1, before the highest relative abundance of *Nannoconus* spp., could be interpreted as a strategy to cope with nutrient-poor conditions in the uppermost part of the water column before installation of oligotrophic stratified waters, and development of *Nannoconus* spp. Stratification of the water column in the Vocontian Basin could be explained by spatial restriction of the basin in a context of sea-level lowstand (Fig. 2). Both very low absolute and relative abundances of boreal/cold-water taxa could be linked to sea-level lowstand preventing migration from high latitudes (Fig. 4).

In the interval corresponding to Unit 2 to upper part of Unit 7 (rest of C2), an increase in surface water trophic levels was supported by increasing both nannofossil fluxes and small placolith abundances. Nannofossil assemblages were well-diversified and absolute abundances of most taxa increase (Fig. 4) suggesting mesotrophic conditions in a large mixing photic zone favourable for the development of a great number of species. However, the deep-dweller nannoconids, recorded a large decrease in their relative abundance, which can correspond to the nannoconid crisis defined by Erba (1994; Fig. 4). Increased input of siliciclastic with respect to the base of the succession, as shown by marly dominant limestone-marlstone alternations, and associated nutrients into the basin, thus promoting nannofossil primary productivity, was probably caused by enhanced runoff from the emergent continents during more humid conditions. These conditions were attested by an increase in proportion of the kaolinite in clay assemblages of the Vocontian Glaise section (Stein et al., 2012; Fig. 2). More available ecological niches relative to sea-level rise (Fig. 2) also explained the greater development of nannoplankton during this time interval. From Units 4 to 7, both absolute and relative abundances of cold taxa (Fig. 4) increased, suggesting connections with higher latitudes, probably due to the transgression. Towards the end of this time interval, increasing abundances of holococcoliths (Fig. 4) could suggest changing nutrient levels in the water column.

The interval spanning from Units 8 to 9 (carbon isotope segments C3–C4), was almost devoid of calcareous nannofossils. A strong dissolution was suspected in this interval as suggested before (Section 5.2), and thus it seems difficult to give interpretations concerning nannofossil primary productivity. It is difficult to interpret maximum value in relative abundance of *Assipetra/Rucinolithus*. Tremolada and Erba (2002) and Erba and Tremolada (2004) suggested that these nannoliths might represent $CaCO_3$ precipitates and/or biocalcification by bacteria under extreme environmental conditions, including methane release induced by volcanic eruption (Opdyke et al., 2001), but it is not possible to discriminate here between primary/preservation signal. Both a maximum in the relative abudance of *Rhagodiscus* spp. (Fig. 4), recorded within the carbon isotope segment C3, and a sharp decrease towards more negative $\delta^{18}O_{carb}$ values concomittant with C3, could be indicative of warmer sea surface waters. Note that a strong positive correlation ($r = 0.75$) was observed between $\delta^{18}O_{carb}$ and $\delta^{13}C_{carb}$ suggesting that diagenesis certainly modified the pristine oxygen isotope composition, and that this record must be interpreted with caution. However, such a trend towards more negative $\delta^{18}O_{carb}$ values was found in many Tethyan settings and in a Pacific site; it is interpreted as "pristine" and indicative of warming (Menegatti et al., 1998; de Gea et al., 2003; Ando et al., 2008; Erba et al., 2010; Kuhnt et al., 2011). In the Cismon section, Keller et al. (2011), on the basis on palynomorph assemblages, recognized that the onset of the warming is concomittant with C3, whereas the thermal maximum was associated with aridity during C4.

From Units 10 to 13 (carbon isotope segments C5–C6, including the "Niveau Goguel"), a weak recovery of nannofossil primary productivity (within C5) was observed, and characterized by increasing abundances of most nannofossil groups, with the exception of holococcoliths and *Nannoconus* spp. whereas this interval corresponded to a maximum in sea-level rise (Fig. 2); absence of *Nannoconus* spp. suggests that environmental conditions in the deep photic zone were not favourable for their development. The top of the succession (Units 14–15, carbon isotope segments C7 and C8) was characterized by a sudden increase in absolute abundances of most nannofossil groups. Nannofossil fluxes and abundances of small placoliths suddenly increased in the lower part of segment C7, indicating a rise in nannofossil primary productivity. Maximum values are then recorded and were indicative of meso-eutrophic conditions, characterizing more stable conditions during a highstand sea-level.

5.4. Time succession in foraminiferal asssemblages at Notre-Dame-de-Rosans

The interval corresponding to carbon isotope segments C3–C6 was characterized by the absence or near absence of planktic foraminifers

which are represented almost exclusively by *G. blowi*. Benthic foraminifers were almost always present but also in few numbers, including Units 11 and 12 of the "Niveau Goguel". However, even if diversity was very low (generally < 12 species) in the first assemblage, it evidenced that bottom waters were not fully anoxic, even in the "Niveau Goguel". Indeed, benthic foraminifers of the morphogroup AG.A. (Ataxophragmids, coiled Lituoilids, Verneuilinids, Eggerellids, Hormosinids…), with a strong dominance of shallow infaunal species, are recognized as having tolerance for oxygen-poor environments (e.g., Koutsouskos and Hart, 1990; Coccioni and Galeotti, 1993; Erbacher et al., 1998, 1999).

Above the "Niveau Goguel" (Unit 14), planktic foraminifers suddenly bloomed. Diversity was high (8 taxa) but the association was dominated by small opportunistic forms. This dramatic change corresponding to the third assemblage could be interpreted as a response to environmental modifications (O_2, salinity) and trophic stratification in the water column. Simple, small morphotypes like Hedbergellids are thought to be ubiquist, ecological opportunists (Hart and Bailey, 1979; Leckie, 1987; Premoli Silva and Sliter, 1995, 1999; Hart, 1999; Keller et al., 2001). The chamber extension of Leupoldinids has been interpreted as an adaptive response to oxygen depletion in the upper water-column, in order to improve oxygen exchanges with seawater as a consequence of the increased surface-area-to-volume ratio (Magniez-Jannin, 1998; Premoli Silva et al., 1999; Bellanca et al., 2002). Eutrophic conditions may have played a significant role in their distribution, together with water oxygenation (Coccioni and Luciani, 2004; Coccioni et al., 2004, 2006). In the same way, benthic foraminifers re-colonized the sea bottom before the end of black shale deposition. Benthic assemblage had a diversity comprised between 15 and 17, and corresponded to morphogroup CH-B3 characterized by Nodosariids, uncoiled Vaginulids, elongate Polymorphinids. Coiled Vaginulids (Astacolus, Lenticulina, Marginulina, Vaginulina) were also present. These species are eurytopic and their occurrence evidences dysaerobic to quasi-anaerobic environments (Koutsouskos and Hart, 1990).

5.5. Origin of TOC-enriched beds at Notre-Dame-de-Rosans and in the Vocontian Basin

The interval represented by grey to black marlstones encompassing the "Niveau Goguel" alternating with siliciclastic turbidites, and containing TOC-enriched beds were observed in Units 11–13 (carbon isotope segments C5–C6). TOC-enriched beds were observed both in the "Niveau Goguel" and above (Fig. 2); they occurred after the onset of the positive excursion in $\delta^{13}C_{carb,}$ started within C4, and disappeared before the end of the positive excursion (Fig. 2). The positive excursion in $\delta^{13}C_{carb}$ recorded in the Early Aptian was generally related to enhanced burial of ^{12}C relative to ^{13}C into sediments due to enhanced primary productivity and concomittant development of dysaerobic to anaerobic conditions, which favoured preservation of organic matter (see Section 1). Results obtained from Rock Eval analyses showed that the Tmax average was around 425 °C indicating that the organic matter did not experience high temperature during burial. Thus, organic matter in the Notre-Dame-de-Rosans section was still immature with respect to petroleum generation. The very low free hydrocarbon content (S1 = 0.03–0.47 mg/g rock) confirmed this immaturity. Such low maturation allowed the use of the hydrogen index (HI) as an indicator of the origin and composition of the organic matter (Espitalié et al., 1985-1986). According to the medium range of HI-values (191–379 mg HC/g TOC) of samples showing TOC > 0.75%, the organic matter of the Notre-Dame-de-Rosans section could be attributed to Type II or to a mixture of Types II and III. Type III is related to terrestrial higher plants debris, whereas Type II is derived mainly from algae and/or bacteria, and generally dominates in dysoxic-anoxic environments. The organic-lean samples contain a Type IV kerogen which is a highly oxidized organic matter. Whereas calcareous nannofossil primary productivity was still low within the "Niveau Goguel" (see Section 5.2), the Type II organic matter detected, could be essentially derived from bacteria. In the Cismon core, the organic matter is predominantly of cyanobacterial origin (Kuypers et al., 2004). Rock Eval and/or organic matter biomarkers analyses conducted on the "Niveau Goguel" in other sections of the Vocontian Basin showed following results: At Serre Chaitieu, organic matter, with TOC up to 2.3%, was mainly of phytoplankton and/or bacterial origin with a very low terrestrial contribution (Heimhofer et al., 2004). The lower part of "Niveau Goguel" was very rich in brilliant and highly fluorescent amorphous organic matter, enriched in inclusions, and interpreted as reflecting dysoxic to anoxic bottom waters, also suggested by a very low bioturbation (Heimhofer et al., 2004). At Glaise, organic matter of Type II (marine origin) was also predominant and associated with the highest TOC values (up to 1.9%). Increase in "redox sensitive" elements remained moderate, indicating dysoxic rather than anoxic bottom waters (Westermann et al., 2013). In the "Niveau Goguel" drilled at Les Sauzeries, the study of biomarkers also revealed an organic matter of marine origin with still a very low contribution of terrestrial matter (Okano et al., 2008). The TOC reached values of 5%. Substantial presence of methyl bacteriohopanepolyol was recorded and would imply a cyanobacterial origin for organic matter (Ando et al., 2013). These cyanobacteria are typical of stratified and oligotrophic waters. In the "Niveau Goguel", the total sulfide content was very high. The level of pyritization was four times higher in the "Niveau Goguel" with respect to the surrounding marlstones and much higher in the lower part of the "Niveau Goguel" than in the upper part (Okano et al., 2008). We have examined nannofacies of sediments drilled at Les Sauzeries, which showed the presence of a large quantity of pyrite both in grey-black marlstones located below the "Niveau Goguel" (Fig. 7A–C), and in the "Niveau Goguel" (Fig. 7D–E). Pyrite richness reflected reducing conditions prevailing in these sediments. Pyrite presented either cube or framboidal forms. This latter form was found in grey-black laminated marlstones and in the "Niveau Goguel" (Fig. 7C–E). Pyrite framboids growth on the surface of sediment deposited in dysoxic bottom waters, where the redox limit is close to the surface of the sediment; the size of framboids is thus comprised between 4 and 50 μm in diameter (Wilkin et al., 1997). Abundant pyrite framboids indicate both high levels of sulphidic production due to intense sulfate reduction by bacteria and dysoxic to anoxic bottom waters (Wilkin and Barnes, 1997; Taylor and Macquaker, 2000; Butler and Rickard, 2000). If the oxygen restriction is even more severe, the redox limit can reach the lower part of the water column and pyrite framboids are then formed in the anoxic and sulfidic water column. The size of these framboids is generally < 6 μm and can be distinguished from framboids of early diagenetic origin. The presence of small-sized framboids in sediments of Les Sauzeries (Fig. 7D–E) suggest an anoxia of the base of the water column within deposition of the "Niveau Goguel" black shales.

5.6. Changes in the carbonate production at Notre-Dame-de-Rosans

At the base of the succession (lower part of the carbon isotope segment C2), deposits were predominantly calcareous dominant limestone-marlstone alternations. Carbonate production was high; nannoconids were the main contributors to the pelagic carbonate fraction, but do not constitute the majority of the carbonate as shown by microfacies observed from thin sections realized in these limestones (Fig. 7F). In most calcareous facies, relative abundance of *Nannoconus* ranged from 30 to 50%. We have investigated more in detail the relationship between nannofossils and calcium carbonate content. In the first graph of the Fig. 6, it is clear that between 25 and 90% of $CaCO_3$, there is a negative correlation between nannofossil absolute abundance and $CaCO_3$%. This suggests that the carbonate fraction was not predominantly produced by calcareous nannofossils, especially for high values of calcium carbonate content (> 70%, Fig. 6). The carbonate fraction was investigated in thin sections of various samples selected

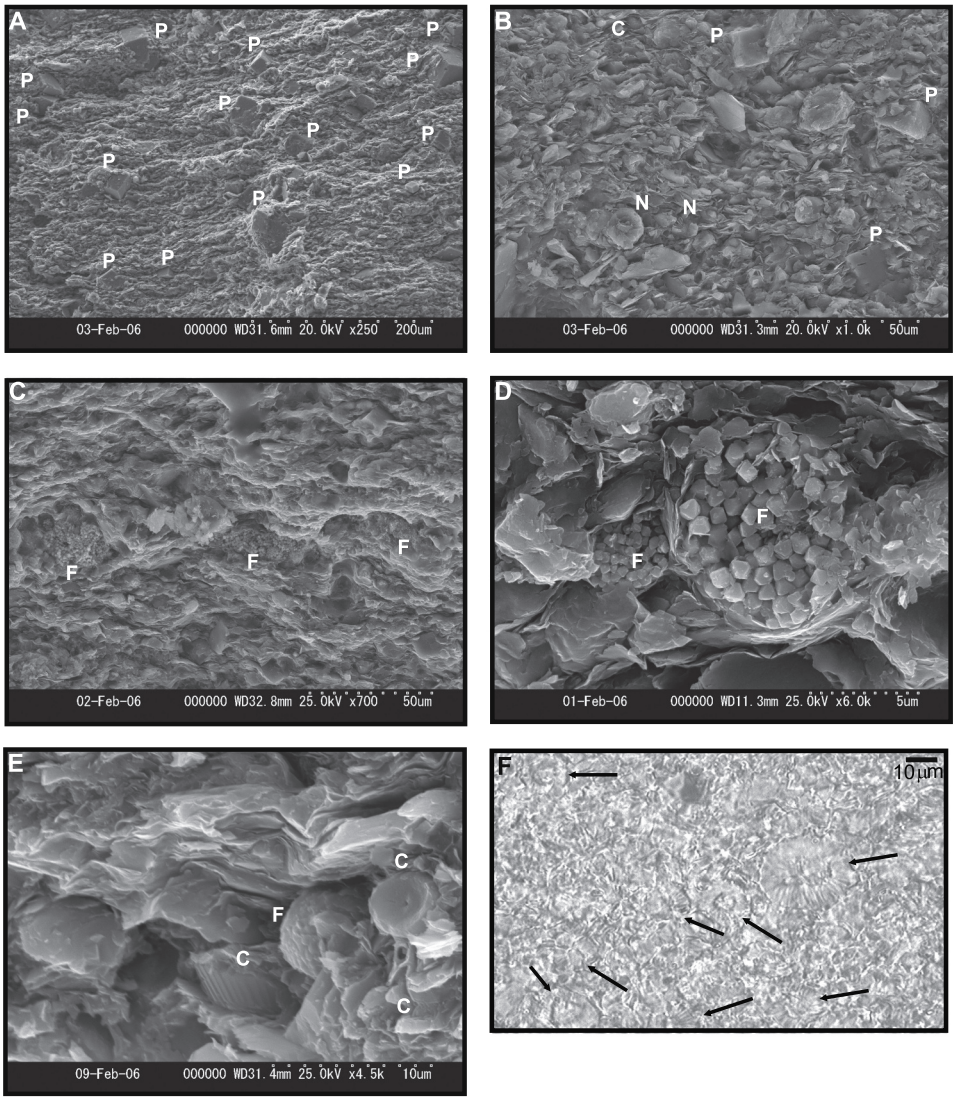

Fig. 7. A–E: Nannofacies SEM pictures of lower Aptian sediments drilled at Les Sauzeries. A–C: in grey-black marls located below the "Niveau Goguel"; D–E: in the "Niveau Goguel"; F: Thin section picture of a lower Aptian limestone bed (unit 1) from the Notre-Dame-de-Rosans section, *Nannoconus* are indicated by black arrows. Abbreviations: C: coccolith; F: framboid; N: *Nannoconus*; P: pyrite.

from different parts of the time interval studied in this work, and from different sections of the Vocontian Basin (including Notre-Dame-de-Rosans) by Bréhéret (1997). He showed that in marlstones located below the "Niveau Goguel" and within this level, planktic foraminifera are rare, whereas in the "Niveau Blanc", which is a biomicrite, planktic foraminifera are abundant and associated with calcispheres and radiolaria. The macrofauna is always rare in all the interval investigated, with only few ammonites. The calciturbidites recognized from Units 2 to 5, present a packstone texture with many bioclasts (benthic foraminifera, miliolids, echinoderms, sponge spicules) derived from surrounding platforms. These observations suggest that for high calcium carbonate values, the carbonate fraction might have a predominantly allochtonous origin, resulting of an export from the carbonate platforms surrounding the Vocontian Basin. On the North Provence platform, for instance, during the same time interval as Unit 1, deposits correspond to the unit U3, which is composed of calcarenites (Masse and Fenerci-Masse, 2011); this unit is considered as partial temporal interval equivalent to the Calcareous Member of the Bedoulian-type series of La Bédoule (Frau et al., 2017). The upper part of the Calcareous Member corresponds to a part of the carbon isotope segment C2 (Lorenzen et al., 2013; Moullade et al., 2015). Progradation of the "Urgonian" platforms towards the basin was maximum during the Barremian-Aptian interval (Ferry and Rubino, 1989). This export occurred during a 3rd order sea-level lowstand (Fig. 2).

The transition from dominant limestone-marlstone alternations to marly dominant limestone-marlstone alternations, intersected by slumps and calcareous bioclastic turbidites (upper part of C2; Fig. 2), marked the first step in decrease in the carbonate production which occurred in two steps at Notre-Dame-de-Rosans. At the top of the dominant limestone-marlstone alternations, the FO of *Rhagodiscus angustus* was recognized (Fig. 2). This FO also occurred at the top of the Calcareous Member in the Bedoulian-type series (Bergen, 1998; Moullade et al., 1998). The change from limestone-to marlstone-dominated sedimentation then occurred during the same time interval both in the Vocontian Basin, and in the South Provençal Basin. At Notre-Dame-de-Rosans, the decrease in $CaCO_3$ content could be due to reduced both export of neritic carbonates from the platforms and pelagic carbonate fraction, since big calcifiers represented by nannoconids recorded a "crisis" as attested by decrease in their relative abundance. On the platforms surrounding the basin, a major sedimentary discontinuity was recorded and occurred within the *Deshayesites forbesi* ammonite Zone (the D3 Mid-Late Bedoulian drowning of Masse and Fenerci-Masse, 2011; Clavel et al., 2013: *D. weissi* ammonite Zone, considered as *D. forbesi* Zone according to the standard zonation of

Reboulet et al. (2011); Pictet et al., 2015; Frau et al., 2017), and within the upper part of the carbon isotope segment C2, taking into account the correlations of platform series with the Bedoulian-type series (Frau et al., 2017) and the carbon isotope stratigraphy of the Bedoulian-type series proposed by Kuhnt et al. (2011), Lorenzen et al. (2013) and Moullade et al. (2015). This major sedimentary discontinuity marked the onset of carbonate platform demise. Following this discontinuity, deposition of argillaceous limestones hemipelagic facies took place on neritic areas surrounding the Vocontian Basin (Masse and Fenerci-Masse, 2011; Clavel et al., 2013; Pictet et al., 2015; Frau et al., 2017). Demise of platforms occurred in a transgressive context (Fig. 2). In this context, the carbonate factory moved towards the margins of the basin and surrounding platforms became narrow fringes with an aggradational rather a progradational pattern (Clavel et al., 2013).

The second drop in the $CaCO_3$ content was drastic and characterized in the lithology by grey to black marly deposits alternating with siliciclastic turbidites (Units 7–10); it was coeval with the negative carbon isotopic shift (C3; Fig. 2). It was followed by a carbonate crash within C4 and C5. The drop could be explained in two ways. It might be related first to the end of export of carbonates from surrounding platforms and resulting replacement of calcareous turbidites by siliciclastic turbidites observed at Notre-Dame-de-Rosans. In a second time (top of C3, Unit 8), the calcium carbonate content dropped to values lower than 5%, with a dramatic decrease in the pelagic carbonate fraction (lowest nannofossil fluxes; Fig. 2) that could be the result of a strong dissolution (see Section 5.2). The end of this interval corresponds to the uppermost part of C5.

Recovery of the carbonate production was progressive and started weakly within C6 (“Niveau Goguel”) up to the top of succession (end of C7; Fig. 2). The carbonate fraction could be mainly of pelagic origin, with the return of nannoconids and the large development of planktic foraminifera (Fig. 2). This time interval was marked by the disappearance of the Urgonian-type platforms around the Vocontian Basin (Pictet et al., 2015). It started first on the North Provence, surrounding the basin southward, with the presence of a sedimentary discontinuity (the D4 Late Bedoulian drowning described by Masse and Fenerci-Masse, 2011). Frau et al. (2017) written that the hiatus materialised by this discontinuity encompassed the “Niveau Goguel”. The lack of sedimentation recorded on the North Provence platform could be related to active tectonics in this area (Frau et al., 2017). Then, on the Ardèche and Vivarais platforms, surrounding the basin westward, another sedimentary discontinuity was observed at the top of the carbon isotope segment C7 (Pictet et al., 2015).

A large increase in the calcium carbonate content was recorded in the “Niveau blanc” (C8; Fig. 2), attributed to the *Dufrenoyia furcata* ammonite Zone by Delamette in Magniez-Jannin et al. (1997) and Dutour (2005). It contained numerous pelycypodes. It represented a shallower depostional environment with respect to its associated with the “Niveau Goguel” (Bréhéret, 1997) and it took place during a 3rd order sea-level lowstand (Ferry and Rubino, 1989).

6. Discussion

6.1. The OAE 1a in the Vocontian Basin: calibration, duration and palaeoceanographic reconstitution

The major environmental perturbation (i.e. dramatic fall in the calcium carbonate content; decrease in nannofossil fluxes, diversity and abundance of most of nannofossil groups; changes in foraminiferal assemblages; Figs. 2–5) spanned from carbon isotope segment C3 to the end of C6 and could correspond to the whole OAE 1a. Deposits, which have the highest organic matter content, characterize the “Niveau Goguel” corresponding to C6, and only representing a part of the OAE 1a.

With regard to the calibration of the OAE 1a with ammonites, data are contradictory between French and Spanish sections. For Moullade et al. (1998), the OAE 1a was dated from the *Roloboceras hambrovi* Subzone, *Deshayesites deshayesi* Zone, whereas for Moreno-Bedmar et al. (2009), it was dated from the *R. hambrovi* Subzone, *D. forbesi* Zone, according to the standard zonation of Reboulet et al. (2011). No ammonites were collected in the Notre-Dame-de-Rosans section. In the Vocontian Basin, the “Niveau Goguel” was attributed to the upper part of the *D. deshayesi* Zone (Delamette in Bréhéret, 1997), which was confirmed by the ammonite biostratigraphic work realized by Dutour (2005) in the Serre Chaitieu section.

The calibration of the OAE 1a with planktic foraminifera showed that this event was located in the *Leupoldina cabri* Zone (Erba et al., 1999). At Notre-Dame-de-Rosans, the “Niveau Goguel” was located in the *Globigerinelloides blowi* Zone. The base of the *L. cabri* Zone was not very well defined in this section due to unfavourable facies for the observation of foraminifera. In other sections of the Vocontian Basin, Magniez-Jannin et al. (1997) observed the first *L. cabri* in the Bedoulian limestone-marlstone alternations which were attributed to the *D. forbesi* ammonite Zone. Some authors defined the base of the *L. cabri* Zone by the acme of this species and not to its first appearance due to very calcareous facies (unfavourable for observation) of the lower Aptian deposits encountered in the Vocontian Basin. This definition of the *L. cabri* Zone was adopted in this study and explains differences of the planktic foraminiferal zonation between southeast France and Cismon in Italy.

The calibration of the OAE 1a with calcareous nannofossils allowed its assignment to the NC6B Subzone at Notre-Dame-de-Rosans. The end of the OAE 1a corresponded to the appearance of the marker *Eprolithus floralis* and the beginning of the NC7 Zone. Several nannofossil bioevents were recognized in this section allowing an accurate biostratigraphic framework across the OAE 1a to be established (Figs. 2 and 8). The succession of nannofossil bioevents observed at Notre-Dame-de-Rosans is 1) entirely consistent with that observed by Erba et al. (1999) in the Cismon core (southern Alps, Italy), 2), consistent with that reported by Herrle and Mutterlose (2003) at Serre Chaitieu (Vocontian Basin, southeast France) from the C4 part since the interval corresponding to C2–C3 is missing, 3) more accurate to those observed by Moullade et al. (2015) in core drillings of Roquefort-La-Bédoule (South Provençal Basin, southeast France), by Aguado et al. (2014) in the Betic Cordillera (southern Spain).

In addition to these nannofossil bioevents, the drastic increase in absolute abundance of *Assipetra/Rucinolithus* during the OAE 1a (within the “Niveau Goguel”) up to the end of the Early Aptian (“Niveau Blanc”) can also be regarded as a useful biostratigraphic marker for the upper Early Aptian in the Vocontian Basin, as already proposed by Herrle and Mutterlose (2003), using their relative abundance. A marked increase in the percentages of this group (especially *A. infracretacea*) above the nannoconid crisis up to the end of the Early Aptian has been recognized in many low latitude settings, and when it is recognized, characterized by increasing abundance of large-sized morphotypes (Erba, 1994; Aguado et al., 1999, 2014; Bergen, 1998; Bralower et al., 1999; Tremolada and Erba, 2002; Herrle and Mutterlose, 2003), but it is not observed in the Notre-Dame-de-Rosans section.

Cyclostratigraphy analysis realized in the Notre-Dame-de-Rosans section allowed the identification of 12 small-scale lithological units and subunits attributed to the 100-kyr cycle of eccentricity, corresponding to a duration of 1200 kyr for the OAE 1a (Fig. 8).

In the Vocontian Basin, the lowermost part of the OAE 1a (lower part of C3) was characterized by a decline in the carbonate content over approximately 100 kyr, which could be attributed to the end of the export of carbonates from surrounding platforms into the basin (Fig. 8). It was followed (upper part of C3 and C4) by a period of maximum oceanographic perturbation on approximately 300 kyr, almost devoid of both phytoplanktic and benthic rests of life (Fig. 8). A strong dissolution was suspected in this interval, but it is difficult to distinguish between dissolution of the carbonate triggered by early diagenetic processes within the pore waters or by ocean acidification. The second hypothesis has already been proposed for other settings with a CO_2-

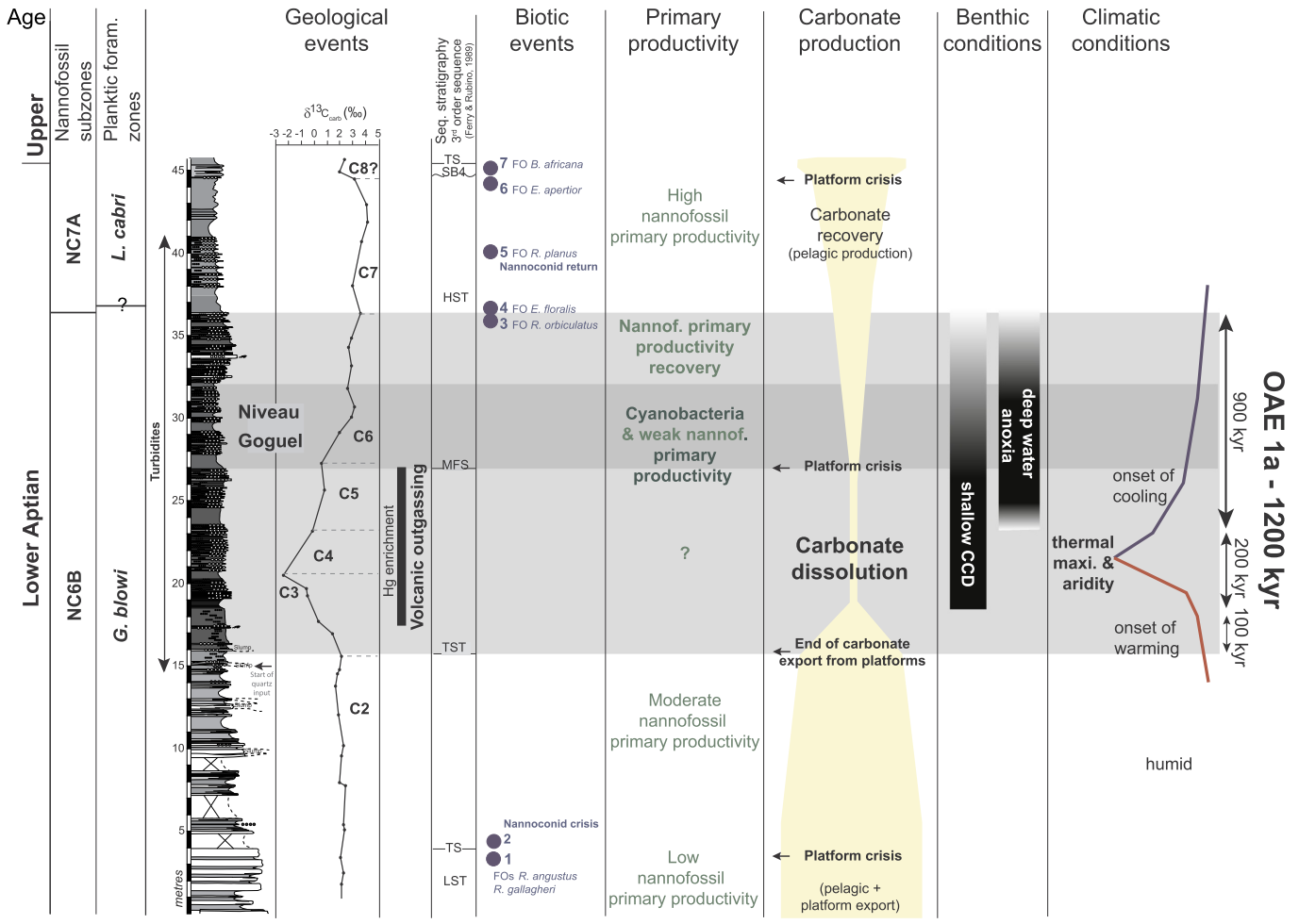

Fig. 8. Synthesis representing biotic changes relative to both palaeoceanographic and climatic variations across the OAE 1a from the Notre-Dame-de-Rosans section.

induced deep ocean acidification which could have a volcanic origin (Erba and Tremolada, 2004; Erba et al., 2010, 2015). Because the main natural source of mercury to the modern environment is volcanic outgassing, Hg/TOC can be used as a volcanic proxy (Sanei et al., 2012). Preliminary Hg/TOC data obtained on the sediments of Notre-Dame-de-Rosans section (Percival et al., 2016) showed that Hg enrichment started within C3 with maximum values recorded in C4 (Fig. 8). Highest values were then recorded below the TOC-enriched beds. Same observations were noticed at Glaise (Vocontian Basin) and La Bédoule (South Provençal Basin) by Charbonnier and Föllmi (2017). These authors concluded that the Hg enrichment cannot be explained by TOC enrichments and corresponding fluctuations in primary productivity and redox conditions, but rather by volcanic outgassing. At Notre-Dame-de-Rosans, Hg enrichment then coincided with the episode of severe dissolution. Increased volcanic CO_2 in the restricted Vocontian Basin could induce both shallowing of the lysocline and presence of acidic waters in the water column.

The upper part of the OAE 1a encompassing black shales of the "Niveau Goguel" and corresponding to C5-base of C7 (800 kyr), was characterized by less severe environmental conditions for marine organisms, with respect to the lower part. The nannofossil primary productivity slowly increased within this part, but remained too weak to produce TOC-enriched beds. The organic matter could be probably derived from cyanobacteria, since biomarkers predominantly of cyanobacterial orgin were detected in the black shales of the "Niveau Goguel" drilled in Les Sauzeries, another setting of the small enclosed Vocontian Basin. Stratified and oligotrophic surface waters prevailed during this time interval, and deep waters were dysoxic to anoxic.

At Notre-Dame-de-Rosans, the onset of the nannoconid crisis was coeval with a step in the "Urgonian" carbonate platform demise, and occurred approximately 500 kyr before the OAE 1a (upper part of C2). Both rise in sea-level and in marine surface water fertility could explain these two crises. This confirms that the onset of this biocalcification crisis was not linked to the OAE 1a, as already suggested by some authors (Naafs et al., 2016).

6.2. Comparison and correlations with other sections

The $\delta^{13}C_{carb}$ signal recorded at Notre-Dame-de-Rosans was very consistent with that recorded at Glaise (Vocontian Basin; Westermann et al., 2013; Fig. 9). In particular, the negative shift attributed to the segment C3 was in the same range of values, with a maximum of −4.5‰ at Notre-Dame-de-Rosans and of −3.9‰ at Glaise. The negative carbon isotope shift recorded in the Vocontian Basin was larger than that recorded in other Tethyan successions (between 0.6 and 1.6‰ in the sections of La Bédoule, 2.6‰ at Cau and 1.2‰ in the Cismon core; Fig. 9), but in the same range than that recorded in the central Pacific Ocean (around 4‰ in the DSDP Site 463; Fig. 9). The C3–C6 interval corresponding to the OAE 1a was more condensed at Notre-Dame-de-Rosans than in the sections of La Bédoule (composite) and Cau, but more dilated than in Cismon (Fig. 9). Black shales of the "Niveau Goguel" were attributed to C6 at Notre-Dame-de-Rosans, to C6–C7 at Serre Chaitieu (Heimhofer et al., 2004), whereas they started within C4 and ended within C7 at Glaise (Westermann et al., 2013). In these Vocontian Basin sections, black shales were only parts of the OAE 1a and were located above the negative shift, as it was observed in the

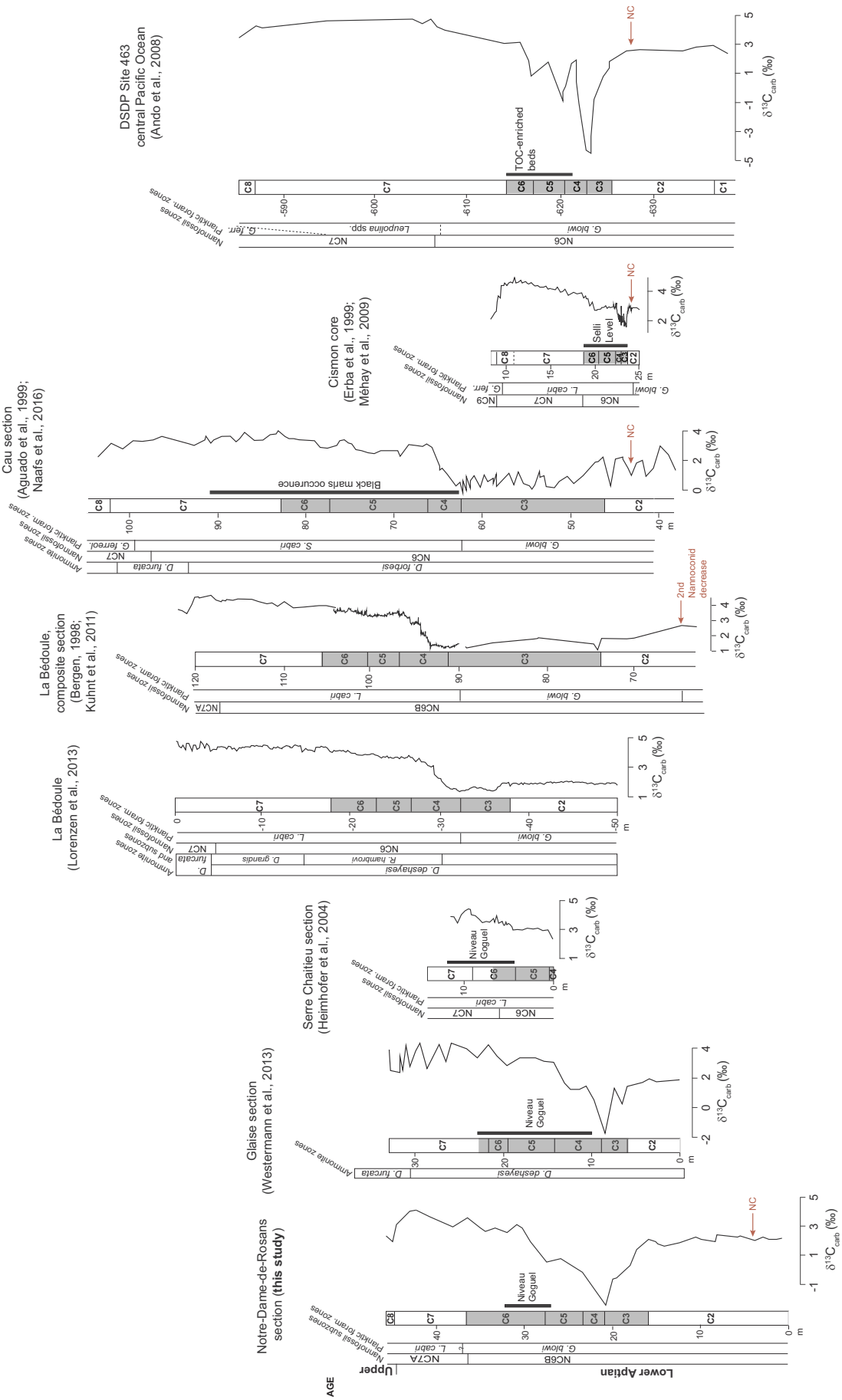

Fig. 9. Comparison of bulk carbon isotope curves from Notre-Dame-de-Rosans section (this work) with other sections of the Vocontian Basin (Glaise and Serre Chaitieu) and with those of La Bédoule (South Provençal Basin, SE France), Cau (southern Spain), Cismon core (southern Alps, Italy) and DSDP Site 463 (central Pacific ocean). The carbon isotope segments as defined by Menegatti et al. (1998), and recognized for all settings, are reported. The grey band corresponds to the stratigraphic extension of the OAE 1a, as reported by the different authors. The black line represents the stratigraphic extension of black shales or TOC-enriched beds when present. NC: Nannoconid crisis.

Cau section (southern Spain; Naafs et al., 2016) where black marls occurred in an interval comprised between C4 and part of C7 (Fig. 9), and in the DSDP Site 463 (Ando et al., 2008) where TOC-enriched beds were recorded at the top of C4 to the end of C6 (Fig. 9). Always in Spain, but in the Subbetic pelagic area, black shales or dark marls were coeval with C3 (XF section) or occurred above the OAE 1a (XF1 section; Aguado et al., 2014). In condensed successions of both the Cismon core and section (southern Alps, Italy), numerous black shale levels characterized the Selli level, that was the expression of the OAE 1a (C3 to C6; Menegatti et al., 1998; Erba et al., 1999; Fig. 9). In the Piobbico core, central Italy, black shales occurred in an interval corresponding to segments C5 to C6 (Bottini et al., 2015; Erba et al., 2015; in this core, the interval below C5 was missing). In other condensed successions such as Roter Sattel (Swiss Romandes Prealps) and DSDP Site 463, black shales corresponded to segments C5 and C4, respectively (Menegatti et al., 1998; Ando et al., 2008).

The onset of the "nannoconid crisis" occurred within the carbon isotope segment C2, and then below the OAE 1a (following the definition of the OAE 1a by Menegatti et al., 1998, as written in the introduction of this work) in the different successions where it was recognized (Fig. 9).

The top of the OAE 1a is well calibrated both with nannofossils and carbon isotopes in the Vocontian Basin (Notre-Dame-de-Rosans and Serre Chaitieu sections) and in the Cismon core; it occurred at the boundary between the nannofossil zones NC6 and NC7 and at the boundary between the chemostratigraphic segments C6 and C7 (Fig. 9). The same calibration was observed for the Piobbico core (central Italy; Erba et al., 2015), and for the DSDP site 398 (North Atlantic; Li et al., 2008). In the Santa Rosa Canyon section (Mexico), and in other Italian successions located in the Gargano Promontory, South Italy (Luciani et al., 2001) and in North-West Sicily (Bellanca et al., 2002), the NC6/NC7 limit occurred within C6 below the top of the OAE 1a. In the South Provençal Basin (Moullade et al., 1998; Kuhnt et al., 2011; Lorenzen et al., 2013; Moullade et al., 2015; Fig. 9), in the Cau section (southern Spain; Aguado et al., 1999; de Gea et al., 2003; Fig. 9), and in the DSDP Site 463 (central Pacific Ocean; Ando et al., 2008), NC6/NC7 limit occurred within C7 above the OAE 1a.

This review showed that black shales were diachronous in the Tethyan realm and characterized only a part of the OAE 1a or all the event.

7. Conclusions

The lower Aptian expanded section of Notre-Dame-de-Rosans located in the Vocontian Basin (southeast France) was investigated with a multidisciplinary approach in order to establish a detailed chronological framework of the main palaeoenvironmental changes occurring across the OAE 1a.

The major environmental perturbation corresponding to the OAE 1a spanned from carbon isotope segment C3 to the end of C6. The richest deposits in organic matter, characterizing the "Niveau Goguel" corresponding to C6, only represented a part of the OAE 1a. The calibration of the OAE 1a with both calcareous nannofossils and planktic foraminifera allowed its assignment to the NC6B Subzone, and to the *Globigerinelloides blowi* Zone, respectively. Several nannofossil bioevents were recognized in the Notre-Dame-de-Rosans section allowing an accurate biostratigraphic framework across the OAE 1a to be established. Cyclostratigraphy analysis allowed us to propose a duration of 1200 kyr for the OAE 1a.

At Notre-Dame-de-Rosans, a stepwise decrease in the carbonate production was recorded. A first decrease corresponded to the onset of the nannoconid crisis into the basin, which was coeval with a step in the "Urgonian" carbonate platform demise; it occurred within the carbon isotope segment C2, approximately 500 kyr before the OAE 1a. Both rise in sea-level and in marine surface water fertility could explain the onset of both neritic and pelagic biocalcification crises. A second decrease, corresponding to a crash in the carbonate content, occurred within C3–C4, 100 kyr after the onset of the OAE 1a event over approximately 300 kyr. It was associated with extremely rare both phytoplanktic and benthic rests of life. A strong dissolution was suspected, possibly due to CO_2-induced ocean acidification. Just before (around 150 kyr) and during the deposition of organic-rich matter layers of the "Niveau Goguel" (400 kyr), anoxia prevailed in deep waters; surface waters primary producers were essentially represented by cyanobacteria, with a small contribution of calcareous nannofossils. Partial recovery of both calcareous nannofossil primary productivity and pelagic carbonate production in surface waters started during the last 300 kyr of the OAE 1a.

This study shows that the onset of both neritic and pelagic carbonate biocalcification crises occurred before the OAE 1a, and are not linked to ocean acidification, as it has already been suggested by previous authors and that black shales and/or organic-rich matter layers were diachronous in the Tethys realm.

Acknowledgments

We are grateful to the editor Thierry Correge, Elisabetta Erba and an anonymous reviewer for both corrections and comments which greatly improved the quality of an earlier version of the manuscript. This study was supported by the projects Monbusho Grant titled «Biological pump and material flux in the hot-house Earth» (PI: H. Okada, Hokkaido University, 2001–2006), and CNRS ECLIPSE II, 2004 and 2005 (PI: B. Pittet). The Laboratories UMR 5275 at the University Grenoble-Alpes and UMR 5276 at the University Lyon 1 are acknowledged. Smear slides and thin sections for calcareous nannofossil analysis are stored in the palaeontological collections de l'Observatoire des Sciences de l'Univers de Grenoble (OSUG); collection numbers are indicated in Appendix A (UJF-ID number).

Appendix A. Supplementary data

Table with the results of the quantitative study in Notre-Dame-de-Rosans section, including $CaCO_3$, TOC and carbon and oxygen isotopes, foraminifera countings, alphabetical list of calcareous nannofossil taxa counted, and percentages of species or group of species both presented in the figures and commented in the manuscript. Supplementary data to this article can be found online at https://doi.org/10.1016/j.palaeo.2018.09.014.

References

Aguado, R., Castro, J.M., Company, M., de Gea, G.A., 1999. Aptian bioevents – an integrated biostrtigraphic analysis of the Almadich Formation, Inner Prebetic Domain, SE Spain. Cretac. Res. 20, 663–683.

Aguado, R., de Gea, G.A., Castro, J.M., O'Dogherty, L., Quijano, M.L., Naafs, B.D.A., Pancost, R.D., 2014. Late Barremian-early Aptian dark facies of the Subbetic (Betic Cordillera, southern Spain): calcareous nannofossil quantitative analyses, chemostratigraphy and palaeoceanographic reconstructions. Palaeogeogr. Palaeoclimatol. Palaeoecol. 395, 198–221.

Ando, A., Kaiho, K., Kawahata, H., Kakegawa, T., 2008. Timing and magnitude of early Aptian extreme warming: unraveling primary δ18O variation in indurated pelagic carbonates at Deep Sea Drilling Project Site 463, central Pacific Ocean. Palaeogeogr. Palaeoclimatol. Palaeoecol. 260, 463–476.

Ando, T., Sawada, K., Takashima, R., Nishi, H., 2013. Paleoproductivity of dinoflagellate and cyanobacteria during the mid-Cretaceous oceanic anoxic events in the Vocontian Basin, SE France. In: 26th IMOG Organic Geochemistry: Trends for the 21st Century. 2. pp. 330–331.

Aubry, M.P., Bord, D., Beaufort, L., Kahn, A., Boyd, S., 2005. Trends in size changes in the coccolithophorids, calcareous nannoplankton, during the Mesozoic: a pilot study. Micropaleontology 51, 309–318.

Beaufort, L., 1991. Adaptation of the random settling method for quantitative studies of calcareous nannofossils. Micropaleontology 37, 415–418.

Bellanca, A., Erba, E., Neri, R., Premoli Silva, I., Sprovieri, M., Tremolada, F., Verga, D., 2002. Palaeoceanographic significance of the Tethyan 'Livello Selli' (early Aptian) from the Hybla Formation, northwestern Sicily: biostratigraphy and high-resolution chemostratigraphic records. Palaeogeogr. Palaeoclimatol. Palaeoecol. 185, 175–196.

Bergen, J.A., 1998. Calcareous nannofossils from the lower Aptian historical stratotype at Cassis-La-Bédoule (SE, France). Géol. Mediterr. 25, 227–255.

Berger, A., Melice, J.L., Loutre, M.F., 2005. On the origin of the 100-kyr cycles in the

astronomical forcing. Paleoceanography 20, PA4019. https://doi.org/10.1029/2005PA001173.
Bersezio, R., Erba, E., Gorza, M., Riva, A., 2002. Berriasian-Aptian black shales of the Maiolica formation (Lombardian Basin, Southern Alps, Northern Italy): local to global events. Palaeogeogr. Palaeoclimatol. Palaeoecol. 180, 253–275.
Bornemann, A., Mutterlose, J., 2006. Size analyses of the coccolith species Biscutum constans and Watznaueria barnesiae from the Late Albian Niveau Breistroffer (SE France): taxonomic and palaeoecological implications. Geobios 39, 599–615.
Bornemann, A., Pross, J., Reichelt, K., Herrle, J.O., Hemleben, C., Mutterlose, J., 2005. Reconstruction of short-term palaeoceanographic changes during the formation of the Late Albian "Niveau Breistroffer" black shales (Oceanic Anoxic Event 1d, SE France). J. Geol. Soc. Lond. 162, 623–639.
Bottini, C., Cohen, A.S., Erba, E., Jenkyns, H.C., Coe, A.L., 2012. Osmium-isotope evidence for volcanism, weathering, and ocean mixing during the early Aptian OAE 1a. Geology 40, 583–586.
Bottini, C., Erba, E., Tiraboschi, D., Jenkyns, H.C., Schiuten, S., Sinninghe Damsté, J.S., 2015. Climate variability and ocean fertility during the Aptian Stage. Clim. Past 11, 383–402.
Bover-Arnal, T., Salas, R., Moreno-Bedmar, J.A., Bitzer, K., 2009. Sequence stratigraphy and architecture of a late Early–Middle Aptian carbonate platform succession from the western Maestrat Basin (Iberian Chain, Spain). Sediment. Geol. 219, 280–301.
Bown, P.R., Rutledge, D.C., Crux, J.A., Gallagher, L.T., 1998. Lower Cretaceous. In: Bown, P.R. (Ed.), Calcareous Nannofossil Biostratigraphy. British Micropalaeontological Society Publications Series Chapman and Hall/Kluwer Academic Publishers, pp. 86–102.
Bralower, T.J., Sliter, W.V., Arthur, M.A., Leckie, R.M., Allard, D., Schlanger, S.O., 1993. Dysoxic/anoxic episodes in the Aptian-Albian (Early Cretaceous). In: Pringle, M.S., Sager, W.W., Sliter, W.V., Stein, S. (Eds.), The Mesozoic Pacific: Geology, Tectonics, and Volcanism, Geophys. Monographic. 77. American Geophysical Union, Washington, DC, pp. 5–37.
Bralower, T.J., Arthur, M.A., Leckie, R.M., Sliter, W.V., Allard, D.J., Schlanger, S.O., 1994. Timing and paleoceanography of oceanic dysoxia/anoxia in the Late Barremian to Early Aptian (Early Cretaceous). PALAIOS 9, 335–369.
Bralower, T.J., Leckie, R.M., Sliter, W.V., Thierstein, H.R., 1995. An integrated Cretaceous microfossil biostratigraphy. SEPM Spec. Publ. 50, 65–79.
Bralower, T.J., CoBabe, E., Clement, B., Sliter, W.V., Osburn, C.L., Longoria, J., 1999. The record of global change in mid-Cretaceous (Barremian-Albian) sections from the Sierra Madre, northeastern Mexico. J. Foraminifer. Res. 29, 418–437.
Brand, L.E., 1994. Physical ecology of marine phytoplankton. In: Winter, A., Siesser, W.G. (Eds.), Coccolithophores. Cambridge University Press, pp. 39–49.
Bréhéret, J.G., 1988. Episodes de sédimentation riches en matière organique dans les marnes bleues d'âge Aptien-Albien de la partie pélagique du bassin vocontien (SE France). Bull. Soc. Geol. Fr. IV, 349–356.
Bréhéret, J.G., 1997. L'Aptien et l'Albien de la fosse vocontienne (des bordures au bassin). Evolution de la sédimentation et enseignements sur les événements anoxiques. Publ. Soc. Geol. Nord 25 (614 pp).
Busson, G., Noël, D., 1991. Les nannoconidés indicateurs environnementaux des oceans et mers épicontinentales du Jurassique terminal et du Crétacé inférieur. Oceanol. Acta 14, 333–356.
Butler, I.B., Rickard, D., 2000. Framboidal pyrite formation via the oxidation of iron (II) monosulphide by hydrogen sulphide. Geochim. Cosmochim. Acta 64, 2665–2672.
Caron, M., 1985. Cretaceous planktic foraminifera. In: Bolli, H.M., Saunders, J.B., Perch-Nielsen, K. (Eds.), Plankton Stratigraphy. Cambridge University Press, pp. 17–86.
Charbonnier, G., Föllmi, K.B., 2017. Mercury enrichments in lower Aptian sediments support the link between Ontong Java large igneous province activity and oceanic anoxic episode 1a. Geology 45, 63–66.
Clavel, B., Conrad, M.A., Busnardo, R., Charollais, J., Granier, B., 2013. Mapping the rise and demise of Urgonian platforms (Late Hauterivian-Early Aptian) in southeastern France and the Swiss Jura. Cretac. Res. 39, 29–46.
Cobianchi, M., Luciani, V., Menegatti, A., 1999. The Selli Level of the Gargano Promontory, Apulia, southern Italy: foraminiferal and calcareous nannofossil data. Cretac. Res. 20, 255–269.
Coccioni, R., Galeotti, S., 1993. Orbitally induced cycles in benthonic foraminiferal morphogroups and trophic structure distribution patterns from the Late Albian "Amadeus Segment" (central Italy). J. Micropalaeontol. 12, 227–239.
Coccioni, R., Luciani, V., 2004. Planktonic foraminifera and environmental changes across the Bonarelli Event (OAE2, latest Cenomanian) in its type area: high-resolution study from the Tethyan reference Bottaccione section (Gubbio, central Italy). J. Foraminifer. Res. 34, 109–129.
Coccioni, R., Erba, E., Premoli Silva, I., 1992. Barremian-Aptian calcareous plankton biostratigraphy from the Gorgo a Cerbara section (Marche, Central Italy) and implication for planktonic evolution. Cretac. Res. 13, 517–537.
Coccioni, R., Luciani, V., Marsili, A., 2004. Cretaceous oceanic anoxic events and radially elongated chambered planktonic foraminifera: paleoecological and paleoceanographic implications. Abstracts. In: 32nd International Geological Congress, Florence, pp. 753.
Coccioni, R., Luciani, V., Marsili, A., 2006. Cretaceous oceanic anoxic events and radially elongated chambered planktonic foraminifera: paleoecological and paleoceanographic implications. Palaeogeogr. Palaeoclimatol. Palaeoecol. 235, 66–92.
Cotillon, P., 1971. Le Crétacé inférieur de l'arc subalpin de Castellane entre l'Asse et le Var. Stratigraphie et sédimentologie. Mém. Bur. Rech. Géol. Min. 68, 1–329 (Orléans).
Cotillon, P., 2010. Sea bottom current activity recorded on the southern margin of the Vocontian basin (southeastern France) during the lower Aptian: evidence for a climatic signal. Bull. Soc. Geol. Fr. 181, 3–18.
Cotillon, P. (coord.), et al., 1984. Crétacé inférieur. In: Debrand-Passart, S. (Ed.), Synthèse géologique du Sud-Est de la France. 125. pp. 287–338 (Mém. du Bur. Rech. Géol. Min., Orléans).
Cotillon, P., Banvillet, M., Gaillard, C., Groshény, D., Olivero, D., 2000. Les surfaces à Rhizocorallium de l'Aptien inférieur de la bordure méridionale du bassin vocontien (France, Sud-Est), marqueurs de dynamiques locales; leur relation avec l'événement anoxique global. Bull. Soc. Geol. Fr. 171, 229–238.
Cros, L., Kleijne, A., Zeltner, A., Billard, C., Young, J., 2000. New examples of holo/heterococcolithophorids combination coccospheres and their implications for coccolihtophorids biology. Mar. Micropaleontol. 39, 1–34.
Crux, J.A., 1989. Biostratigraphy and palaeogeographical applications of Lower Cretaceous nannofossils from northwestern Europe. In: Crux, J.A., van Heck, S.E. (Eds.), Nannofossils and Their Applications. Ellis Horwood, Chichester, pp. 143–211.
Crux, J.A., 1991. Albian calcareous nannofossils from the Gault Clay of Munday's Hill (Bedforshire, England). J. Micropalaeontol. 10, 203–221.
D'Argenio, B., Ferreri, V., Weissert, H., Amodio, S., Buonocunto, F.P., Wissler, L., 2004. A multidisciplinary approach to global correlation and geochronology. The Cretaceous shallow-water carbonates of Southern Apennines, Italy. In: D'Argenio, B., Fischer, A.G., Premoli Silva, I., Weissert, H., Ferreri, V. (Eds.), Cyclostratigraphy; Approaches and Cases Histories. SEPM Spec. Publ 81. pp. 103–122.
de Gea, G.A., Castro, J.M., Aguado, R., Ruiz-Ortiz, P.A., Company, M., 2003. Lower Aptian carbon isotope stratigraphy from a distal carbonate shelf setting: the Cau section, Prebetic zone, SE Spain. Palaeogeogr. Palaeoclimatol. Palaeoecol. 200, 207–219.
Dutour, Y., 2005. Biostratigraphie, evolution et renouvellements des ammonites de l'Aptien supérieur (Gargasien) du bassin vocontien (Sud-Est de la France). 1 Univ. Lyon (Unpublished PhD thesis), 302 pp.
Erba, E., 1987. Mid-Cretaceous cyclic pelagic facies from the Umbrian- Marchean Basin: what do calcareous nannofossils suggest? Int. Nannoplankton Assoc. Newsl. 9, 52–53.
Erba, E., 1992. Middle Cretaceous calcareous nannofossils from the western Pacific (Leg 129): evidence for paleoequatorial crossings. In: Larson, R.L., Lancelot, Y. (Eds.), Proceedings of the Ocean Drilling Program. Scientific Results Vol. 129. pp. 189–201.
Erba, E., 1994. Nannofossils and superplumes: the early Aptian "nannoconid crisis". Paleoceanography 9, 483–501.
Erba, E., 1996. The Aptian stage. Bull. Inst. Royal Sci. Nat. Belg. 66, 31–43.
Erba, E., 2004. Calcareous nannofossils and Mesozoic oceanic anoxic events. Mar. Micropaleontol 52, 85–106.
Erba, E., Tremolada, F., 2004. Nannofossil carbonate fluxes during the Early Cretaceous: phytoplankton response to nutrification episodes, atmospheric CO_2 and anoxia. Paleoceanography 19, 1–18.
Erba, E., Guasti, G., Castradori, D., 1989. Calcareous nannofossils record fertility and temperature cycles: evidence from the Albian Gault Clay Formation. INA Newslett. 11, 57–58.
Erba, E., Castradori, D., Guasti, G., Ripepe, M., 1992. Calcareous nannofossils and Milankovitch cycles: the example of the Albian Gault Clay Formation (southern England). Palaeogeogr. Palaeoclimatol. Palaeoecol. 93, 47–69.
Erba, E., Channell, J.E.T., Claps, M., Jones, C., Larson, R.L., Opdyke, B., Premoli Silva, I., Riva, A., Salvini, G., Torricelli, S., 1999. Integrated stratigraphy of the Cismon Apticore (Southern Alps, Italy): a reference section for the Barremian-Aptian interval at low latitudes. J. Foraminifer. Res. 29, 371–391.
Erba, E., Bottini, C., Weissert, J.H., Keller, C.E., 2010. Calcareous nannoplankton response to surface-water acidification around oceanic anoxic event 1a. Science 329, 428–432.
Erba, E., Duncan, R.A., Bottini, C., Tiraboschi, D., Weissert, H., Jenkyns, H.C., Malinverno, A., 2015. Environmental consequences of Ontong Java Plateau and Kerguelen Plateau volcanism. Geol. Soc. Am. Spec. Pap. 511. https://doi.org/10.1130/2015.2511(15).
Erbacher, J., Thurow, J., Littke, R., 1996. Evolution patterns of radiolarian and organic matter variations: a new approach to identify sea-level changes in mid-Cretaceous pelagic environments. Geology 24, 499–502.
Erbacher, J., Gert, W., Schmiedl, G., Hemleben, C., 1998. Benthic foraminiferal assemblages of late Aptianeearly Albian black shale intervals from the Vocontian Basin, SE France. Cretac. Res. 19, 805–826.
Erbacher, J., Hemleben, C., Huber, B.T., Markey, M., 1999. Correlating environmental changes during early Albian oceanic anoxic event 1B using benthic foraminifera paleoecology. Mar. Micropaleontol. 38, 7–28.
Espitalié, J., Deroo, G., Marquis, F., 1985-1986. La pyrolyse Rock-Eval et ses applications. Rev. Inst. Fr. Pétrol. 40 (1985), 563–579 (755-784; 41 (1986), 73-89).
Ferry, S., Rubino, J.-L., 1989. Mesozoic eustacy record on western Tethyan margins. Post-meeting field-trip in the Vocontian Trough. Publ. Assoc. Sedim. Fr. 12 (141pp).
Flandrin, J., 1963. Remarques stratigraphiques, paléontologiques et structurales sur la region de Séderon. Bull. Serv. Carte Géol. Fr. 272, 815–845.
Föllmi, K.B., 2012. Early Cretaceous life, climate and anoxia. Cretac. Res. 35, 230–257.
Frau, C., Pictet, A., Spangenberg, J.E., Masse, J.-P., Tendil, A.J.-B., Lanteaume, C., 2017. New insights on the age of the post-Urgonian marly cover of the Apt region (Vaucluse, SE France) and its implications on the demise of the North Provence carbonate platform. Sediment. Geol. 359, 44–61.
Friès, G., 1987. Dynamique du basin subalpine meridional de l'Aptien au Cénomanien. 4 Sci. Université Paris Vi, 1986. Mém. Sci. Terre Ecole des Mines de Paris (Thèse Doct., 370 pp).
Friès, G., Parize, O., 2003. Anatomy of ancient passive margin slope systems: Aptian gravity-driven deposition on the Vocontian palaeomargin, western Alps, south-east France. Sedimentology 50, 1231–1270.
Friès, G., Beaudoin, B., Joseph, Ph., Patemoster, B., 1984. Les "Grès de Rosans" et les slumpings aptiens associés: restitution paléomorphologique. Bull. Soc. Geol. Fr. 26, 693–702.
Geisen, M., Bollmann, J., Herrle, J.O., Mutterlose, J., Young, J.R., 1999. Calibration of the random settling technique for calculation of absolute abundances of calcareous nannoplankton. Micropalaeontology 45, 437–442.
Ghirardi, J., Deconinck, J.-F., Pellenard, P., Martinez, M., Bruneau, L., Amiotte-Suchet, P., Pucéat, E., 2014. Multi-proxy orbital chronology in the aftermath of the Aptian Oceanic Anoxic Event 1a: palaeoceanographic implications (Serre Chaitieu section, Vocontian Basin, SE France). Newsl. Stratigr. 47, 247–262.
Giraud, F., Olivero, D., Baudin, F., Reboulet, S., Pittet, B., Proux, O., 2003. Minor changes in surface water fertility across the Oceanic Anoxic Event 1d (latest Albian, SE France) evidenced by calcareous nannofossils. Int. J. Earth Sci. 92, 267–284.

Hart, M.B., 1999. The evolution and biodiversity of Cretaceous Planktonic Foraminiferida. Geobios 32, 247–255.
Hart, M.B., Bailey, H.W., 1979. The distribution of planktonic Foraminiferida in the Mid-Cretaceous of NW Europe. In: Wiedmann, J. (Ed.), Aspekte der Kreide Europas. Int. Union Geol. Sci., Ser. A 6. pp. 527–542.
Haworth, M., Hesselbo, S.P., McElwain, J.C., Robinson, S.A., Brunt, J.W., 2005. Mid-cretaceous pCO2 based on stomata of the extinct conifer Pseudofrenelopsis (Cheirolepidiaceae). Geology 33, 749–752.
Heimhofer, U., Hochuli, P.A., Herrle, J.O., Andersen, N., Weissert, H., 2004. Absence of major vegetation and palaeoatmospheric pCO2 changes associated with oceanic anoxic event 1a (Early Aptian, SE France). Earth Planet. Sci. Lett. 223, 303–318.
Heimhofer, U., Hochuli, P.A., Herrle, J.O., Weissert, H., 2006. Contrasting origins of Early Cretaceous black shales in the Vocontian Basin: evidence from palynological and calcareous nannofossil records. Palaeogeogr. Palaeoclimatol. Palaeoecol. 235, 93–109.
Herrle, J.O., 2002. Mid-Cretaceous Paleoceanographic and Paleoclimatologic Implications on Black Shale Formation of the Vocontian Basin and Atlantic. Evidence From Calcareous Nannofossils and Stable Isotopes. 27 Institut und Museum für Geologie und Paläontologie der Universität Tubingen (114 pp).
Herrle, J.O., 2003. Reconstructing nutricline dynamics of mid-Cretaceous oceans: evidence from calcareous nannofossils from the Niveau Paquier black shale (SE France). Mar. Micropaleontol. 47, 307–321.
Herrle, J.O., Mutterlose, J., 2003. Calcareous nannofossils from the Aptian-early Albian of SE France: paleoecological and biostratigraphic implications. Cretac. Res. 24, 1–22.
Herrle, J.O., Kössler, P., Friedrich, O., Erlenkeuser, H., Hemleben, C., 2004. High resolution carbon isotope records of the Aptian to lower Albian from SE France and the Mazagan Plateau (DSDP Site 545). A stratigraphic tool for paleoceanographic and paleobiologic reconstruction. Earth Planet. Sci. Lett. 218, 149–161.
Hibsch, C., Jandel, D., Montenat, C., Ott d'Estevou, P., 1992. Evénements tectoniques crétacés dans la partie méridionale du bassin subalpine (massif Ventoux-Lure et partie orientale de l'arc de Castellane, SE France). Implications géodynamiques. Bull. Soc. Geol. Fr. 163, 147–158.
Hill, M.E., 1975. Selective dissolution of mid-Cretaceous (Cenomanian) calcareous nannofossils. Micropaleontology 21, 227–235.
Hong, S.K., Lee, Y.I., 2012. Evaluation of atmospheric carbon dioxide concentrations during the Cretaceous. Earth Planet. Sci. Lett. 328-327, 23–28.
Hu, X., Kuidong, Z., Yilmaz, I.O., Yongxiang, L., 2012. Stratigraphic transition and palaeoenvironmental changes from the Aptian oceanic anoxic event 1a (OAE 1a) to the oceanic red bed 1 (ORB1) in the Yenicesihlar section, central Turkey. Cretac. Res. 38, 40–51.
Huang, C., Hinnov, L., Fischer, A.G., Grippo, A., Herbert, T., 2010. Astronomical tuning of the Aptian Stage from Italian reference sections. Geology 38, 899–902.
Huck, S., Heimhofer, U., Rameil, N., Bodin, S., Immenhauser, A., 2011. Strontium and carbon-isotope chronostratigraphy of Barremian-Aptian shoal-water carbonates: Northern Tethyan platform drowning predates OAE 1a. Earth Planet. Sci. Lett. 304, 547–558.
Jahren, A.H., Arens, N.C., Sarmiento, G., Guerrero, J., Amundson, R., 2001. Terrestrial record of methane hydrate dissociation in the Early Cretaceous. Geology 29, 159–162.
Jenkyns, H.C., 1995. Carbon-isotope stratigraphy and palaeoceanographic significance of the lower Cretaceous shallow water carbonates of Resolution Guyot. In: Winterer, E.L., Sager, W.W., Firth, J.V., Sinton, J.M. (Eds.), Proceedings of the Ocean Drilling Program, Scientific Results. 143. Ocean Drilling Program, College Station, TX, pp. 99–104.
Jenkyns, H.C., 2010. Geochemistry of oceanic anoxic events. Geochem. Geophys. Geosyst. 11. https://doi.org/10.1029/2009GC002788.
Kandel, D., 1992. Analyse paléotectonique de la plate-forme méridionale du bassin vocontien et de ses bordures, durant l'intervalle barrémo-albien (Ventoux-Lure-Baronnies, Chaînes subalpines méridionales, France). Thèse. Univ. Paris VI, pp. 1–323.
Keller, G., Han, Q., Adatte, T., Burns, S.J., 2001. Palaeoenvironment of the Cenomanian-Turonian transition at Eastbourne, England. Cretac. Res. 22, 391–422.
Keller, C.E., Hochuli, P.A., Weissert, H., Bernasconi, S.M., Giorgioni, M., Garcia, T.I., 2011. A volcanically induced climate warming and floral change preceded the onset of OAE1a (Early Cretaceous). Palaeogeogr. Palaeoclimatol. Palaeoecol. 305, 43–49.
Kleijne, A., 1991. Holococcolithophorids from the Indian Ocean, Red Sea, Mediterranean Sea and North Atlantic Ocean. Mar Micropaleont. 17, 1–76.
Koutsouskos, E.A.M., Hart, M.B., 1990. Cretaceous foraminiferal morphogroup distribution patterns, palaeocommunities and trophic structures: a case study from the Sergipe basin, Brazil. Trans. Roy. Soc. Edinb. Earth Sci. 81, 221–246.
Kuhnt, W., Holbourn, A., Moullade, M., 2011. Transient global cooling at the onset of early Aptian oceanic anoxic event (OAE) 1a. Geology 39, 323–326.
Kuypers, M.M.M., Van Breugel, Y., Schouten, S., Erba, E., Sinninghe Damsté, J.S., 2004. N_2-fixing cyanobacteria supplied nutrient N fro Cretaceous oceanic anoxic events. Geology 32, 853–856.
Larson, R.L., Erba, E., 1999. Onset of the mid-Cretaceous greenhouse in the Barremian-Aptian: igneous events and the biological, sedimentary and geochemical responses. Paleoceanography 14, 663–678.
Leckie, R.M., 1987. Palaeoecology of mid-Cretaceous planktonic foraminifera: a comparison of open ocean and epicontinental sea assemblages. Micropaleontology 33, 164–176.
Leckie, R.M., Bralower, T.J., Cashman, R., 2002. Oceanic anoxic events and plankton evolution: biotic response to tectonic forcing during the mid-Cretaceous. Paleoceanography 17, 13–29.
Lees, J.A., Bown, P.R., Young, J.R., Riding, J.B., 2004. Evidence for annual records of phytoplankton productivity in the Kimmeridge Clay Formation coccolith stone bands (Upper Jurassic, Dorset, UK). Mar. Micropaleontol. 52, 29–49.
Lees, J.A., Bown, P.R., Mattioli, E., 2005. Problems with proxies? Cautionary tales of calcareous nannofossil paleoenvironmental indicators. Micropaleontology 51, 333–343.
Lees, J.A., Bown, P.R., Young, J.R., 2006. Photic zone palaeoenvironments of the Kimmeridge Clay Formation (Upper Jurassic, UK) suggested by calcareous nannoplankton palaeoecology. Palaeogeogr. Palaeoclimatol. Palaeoecol. 235, 110–134.
Li, Y.-X., Bralower, T.J., Montañez, I.P., Osleger, D.A., Arthur, M.A., Bice, D.M., Herbert, T.D., Erba, E., Premoli Silva, I., 2008. Toward an orbital chronology for the early Aptian Oceanic Anoxic Event (OAE1a, 120 Ma). Earth Planet. Sci. Lett. 271, 88–100.
Linnert, C., Mutterlose, J., Erbacher, J., 2010. Calcareous nannofossils of the Cenomanian/Turonian boundary interval from the Boreal Realm (Wunstorf, northwest Germany). Mar. Micropaleontol. 74, 38–58.
Loeblich, A.R., Tappan, H., 1988. Foraminiferal Genera and Their Classification. Van Nostrand Reinhold, New York.
Lorenzen, J., Kuhnt, W., Holbourn, A., Flögel, S., Moullade, M., Tronchetti, G., 2013. A new sediment core from the Bedoulian (Lower Aptian) stratotype at Roquefort-La Bédoule, SE France. Cretac. Res. 39, 6–16.
Luciani, V., Cobianchi, M., Jenkyns, H.C., 2001. Biotic and geochemical response to anoxic events: the Aptian pelagic succession of the Gargano Promontory (southern Italy). Geol. Mag. 138 (277–298), 2001.
Luciani, V., Cobianchi, M., Lupi, C., 2006. Regional record of a global oceanic anoxic event: OAE1a on the Apulia Platform margin, Gargano Promontory, southern Italy. Cretac. Res. 27, 754–772.
Magniez-Jannin, F., 1998. L'élongation des loges chez les foraminifères planctoniques du Crétacé inférieur: une adaptation à la sous-oxygénation des eaux? CRAS Sci. Terre 326, 207–213.
Magniez-Jannin, F., Bréhéret, J.G., Delanoy, G., 1997. Un exemple de spéciation lié à l'eustatisme : l'apparition précoce de Schackoina cabri (foraminifère planctonique mésogéen). CRAS Sci. Terre 325, 225–230.
Malinverno, A., Erba, E., Herbert, T.D., 2010. Orbital tuning as an inverse problem: chronology of the early Aptian oceanic anoxic event 1a (Selli Level) in the Cismon APTICORE. Paleoceanography 25, PA2203. https://doi.org/10.1029/2009PA001769.
Masse, J.-P., Fenerci-Masse, M., 2011. Drowning discontinuities and stratigraphic correlation in platform carbonates. The late Barremian-Early Aptian record of southeast France. Cretac. Res. 32, 659–684.
Masse, J.P., Philip, J., 1976. Paléogéographie et tectonique du Crétacé moyen en Provence: révision du concept d'isthme durancien. Rev. Géogr. Phys. Géol. Dyn. 18, 49–66.
Masse, J.-P., Bouaziz, S., Amon, E.Q., Baraboshkin, E., Takorwski, R., Bergerat, F., Sandulescu, M., Platel, J.-P., Canérot, J., Guiraud, R., Poisson, A., Ziegler, M., Rimmele, G., Vrielynck, B., 2000. Map 13 - Early Aptian (114–112 Ma). In: Dercourt, J., Gaetani, M., Vrielynck, B., Barrier, E., Biju-Duval, B., Brunet, M.-F., Cadet, J.-P., Crasquin, S., Sandulescu, M. (Eds.), Atlas Peri-Tethys, Palaeogeographical Maps. Commission de la Carte Géologique du Monde/Commission for the Geological Map of the World (CCGM/CGMW), Paris, 24 Maps, Explanatory Notes I-XX, (269 p).
Mattioli, E., Pittet, B., Riquier, L., Grossi, V., 2014. The mid-Valanginian Weissert Event as recorded by calcareous nannoplankton in the Vocontian Basin. Palaeogeogr. Palaeoclimatol. Palaeoecol. 414, 472–485.
Méhay, S., Keller, C.E., Bernasconi, S.M., Weissert, H., Erba, E., Bottini, C., Hochuli, P.A., 2009. A volcanic CO2 pulse triggered the Cretaceous Oceanic Anoxic Event 1a and a biocalcification crisis. Geology 37, 819–822.
Melinte, M., Mutterlose, J., 2001. A Valanginian (Early Cretaceous), boreal nannoplankton excursion in sections from Romania. Mar. Micropaleontol. 43, 1–25.
Menegatti, A.P., Weissert, H., Brown, R.S., Tyson, R.V., Farrimond, P., Strasser, A., Caron, M., 1998. High-resolution $\delta^{13}C$ stratigraphy through the early Aptian "Livello Selli" of the Alpine Tethys. Paleoceanography 13, 530–545.
Moreno-Bedmar, J.A., Company, M., Bover-Arnal, T., Salas, R., Delanoy, G., Martinez, R., Grauges, A., 2009. Biostratigraphic c haracterization by means of ammonoids of the lower Aptian Oceanic Anoxic Event (OAE 1a) in the eastern Iberian Chain (Maestrat Basin, eastern Spain). Cretac. Res. 30, 864–872.
Moullade, M., Tronchetti, G., Busnardo, R., Masse, J., 1998. Description lithologique des coupes types du stratotype historique de l'Aptien inférieur dans la region de Cassis-La Bedoule (SE France). Géol. Mediterr. 25, 25–29.
Moullade, M., Tronchetti, G., Granier, B., Bornemann, A., Kuhnt, W., Lorenzen, J., 2015. High-resolution integrated stratigraphy of the OAE 1a and enclosing strata from core drillings in the Bedoulian stratotype (Roquefort-La-Bédoule, SE France). Cretac. Res. 56, 119–140.
Mutterlose, J., 1989. Temperature-controlled migration of calcareous nannofloras in the north-west European Aptian. In: Crux, J.A., van Heck, S.E. (Eds.), Nannofossils and Their Applications. Ellis Horwood, Chichester, pp. 122–142.
Mutterlose, J., 1991. Das Verteilungs-und Migrationsmuter des kalkigen Nannoplanktons in der borealen Unter-Kreide (Valangin-Apt) NW-Deutschlands. Palaeontographica B221, 27–152.
Mutterlose, J., 1992. Biostratigraphy and palaeobiogeography of Early Cretaceous calcareous nannofossils. Cretac. Res. 13, 167–189.
Mutterlose, J., Kessels, K., 2000. Early cretaceous calcareous nannofossils from high latitudes: implications for palaeobiogeography and palaeoclimate. Palaeogeogr. Palaeoclimatol. Palaeoecol. 160, 347–372.
Mutterlose, J., Wise, S.W., 1990. Lower Cretaceous nannofossil biostratigraphy of ODP Leg 113 Holes 692B and 693A, continental slope off east Antarctica, Weddell Sea. In: Barker, P.F., Kennett, J.P. (Eds.), Proc. ODP, Sci. Results 113 College Station, TX (Ocean Drilling Program).
Mutterlose, J., Brumsack, H., Flögel, S., Hay, W., Klein, C., Langrock, U., Lipinski, M., Ricken, W., Söding, E., Stein, R., Swientek, O., 2003. The Greenland-Norwegian Seaway: a key area for understandin Late Jurassic to Early Cretaceous paleoenvironments. Paleoceanography 18, 1–26.
Naafs, B.D.A., Castro, J.M., De Gea, G.A., Quijano, M.L., Schmidt, D.N., Pancost, R.D., 2016. Gradual and sustained carbon dioxide release during Aptian Oceanic Anoxic Event 1a. Nat. Geosci. 9, 135–139.
Okada, H., McIntyre, A., 1977. Modern coccolithophores of the Pacific and North Atlantic Oceans. Micropaleontology 23, 1–55.
Okano, K., Sawada, K., Takashima, R., Nishi, H., Okada, H., 2008. Depositional

environments revealed from biomarkers in sediments deposited during the Mid-Cretaceous Oceanic Anoxic events (OAEs) in the Vocontian Basin (SE France). In: Okada, H., Mawatari, S.F., Suzuki, N., Gautam, P. (Eds.), Origin and Evolution of Natural Diversity, Proceedings of International Symposium, 1–5 October 2007, Sapporo, pp. 233–238.
Opdyke, B., Erba, E., Larson, R., Herbert, T., 2001. Hot LIPs, methane and carbon isotope history of the Apticore. Abstracts. J. Conf. EUG XI. EVO5 6, 203.
Pauly, S., Mutterlose, J., Alsen, P., 2012. Lower Cretaceous (upper Ryazanian-Hauterivian) chronostratigraphy of high latitudes (North-Esat Greenland). Cretac. Res. 34, 308–326.
Perch-Nielsen, K., 1985. Mesozoic calcareous nannofossils. In: Bolli, H.M., Saunders, J.B., Perch-Nielsen, K. (Eds.), Plankton Stratigraphy. Cambridge University Press, Cambridge, pp. 329–426.
Percival, L., Jenkyns, H.C., Mather, T.A., Hesselbo, S.P., Ruhl, M., Tedeschi, L.R., Whiteside, J.H., Woelders, L., Giraud, F., Pittet, B., Grosheny, D., Baudin, F., Reboulet, S., 2016. Mercury as a Proxy for Large Igneous Province Volcanism: A Comparison of Mesozoic Events. American Geophysical Union, Fall General Assembly 2016, Abstract id. V34B-01.
Peybernès, C., Giraud, F., Jaillard, E., Robert, E., Masrour, M., Aoutem, M., Içame, N., 2013. Stratigraphic framework and calcareous nannofossil productivity of the Essaouira-Agadir Basin (Morocco) during the Aptian-EarlyAlbian: comparison with the north Tethyan margin. Cretac. Res. 39, 149–169.
Pictet, A., Delanoy, G., Adatte, T., Spangenberg, J.E., Baudouin, C., Boselli, P., Boselli, M., Föllmi, K.B., 2015. Three successive phases of platform demise during the early Aptian and their association with the oceanic anoxic Selli episode (Ardèche, France). Palaeogeogr. Palaeoclimatol. Palaeoecol. 418, 101–125.
Pittet, B., Van Buchem, F.S.P., Hillgärtner, H., Razin, P., Grötsch, J., Droste, H., 2002. Ecological succession, palaeoenvironmental change, and depositional sequences of Barremian–Aptian shallow-water carbonates in northern Oman. Sedimentology 49, 555–581.
Posamentier, H.W., Vail, P.R., 1988. Eustatic controls on clastic deposition II – sequence and systems tract models. In: Wilgus, C.K., Hastings, B.S., Kendall, C.G.St.C., Posamentier, H.W., Ross, C.A., Van Wagoner, J.C. (Eds.), Sea Level Changes: An Integrated Approach. 42. SEPM, Special Publication, pp. 125–154.
Premoli Silva, I., Sliter, W.V., 1995. Cretaceous planktonic foraminiferal biostratigraphy and evolutionary trends from the Bottacione section, Gubbio, Italy. Palaeont. Ital. 82, 1–89.
Premoli Silva, I., Sliter, W.V., 1999. Cretaceous palaeoceanography: evidence for planktonic foraminiferal evolution. Geol. Soc. Am. Spec. Pap. 332, 301–328.
Premoli Silva, I., Erba, E., Tornaghi, M.E., 1989. Paleoenvironmental signals and changes in surface fertility in Mid Cretaceous Corg-rich pelagic facies of the Fucoid Marls (Central Italy). Geobios 11, 225–236.
Premoli Silva, I., Erba, E., Salvini, G., Verga, D., Locatelli, C., 1999. Biotic changes in cretaceous anoxic events. J. Foraminifer. Res. 29, 352–370.
Razin, P., Grelaud, C., van Buchem, F., 2017. The mid-Cretaceous Natih Formation in Oman: a model for cabonate platforms and organic-rich intrashelf basins. AAPG Bull. 101, 512–522.
Reboulet, S., Rawson, P.F., Moreno-Bedmar, J.A. (reporters), et al., 2011. Report on the 4th international meeting of the IUGS Lower Cretaceous Ammonite Working Group, the “Kilian Group” (Dijon, France, 30th August 2010). Cretac. Res. 32, 786–793 (20 co-authors).
Renaud, S., Klaas, C., 2001. Seasonal variations in the morphology of the coccolithophore *Calcidiscus leptoporus* off Bermuda (N. Atlantic). J. Plankton Res. 23, 779–795.
Ricou, L.E., Frizon de Lamotte, D., 1986. Décrochements sénestresmédio-crétacés entre Provence et Alpes-Maritimes (Alpes occidentales, France). Rev. Géol. Dynam. Géog. Phys. 27, 237–245.
Robaszynski, F., Caron, M., 1995. Foraminifères planctoniques du Crétacé: commentaire de la zonation europe-méditerranée. Bull. Soc. Geol. Fr. 166, 681–692.
Robaszynski, F., Caron, M., Groupe de travail européen des foraminifères planctoniques, 1979. Atlas des foraminifères planctoniques du Crétacé moyen (Mer boréale et Téthys). Cah. Micropaleontol. 1, 185–2, 181.
Roth, P.H., 1978. Cretaceous nannoplankton biostratigraphy and oceanography of the northwestern Atlantic Ocean. In: Benson, W.E., Sheridan, R.E. (Eds.), Initial Reports of the Deep Sea Drilling Project. 44. pp. 731–760.
Roth, P.H., 1981. Mid-Cretaceous calcareous nannoplankton from the Central Pacific: implications for paleoceanography. In: Thiede, J. (Ed.), Initial Reports of the Deep Sea Drilling Project. 62. pp. 471–489.
Roth, P.H., 1983. Jurassic and Lower Cretaceous calcareous nannofossils in the western North Atlantic (Site 534): biostratigraphy, preservation, and some observations on biogeography and paleoceanography. In: Sheridan, R.E., Gradstein, F.M. (Eds.), Initial Reports of the Deep Sea Drilling Project. 76. U.S. Government Printing Office, Washington, pp. 587–621.
Roth, P.H., 1986. Mesozoic palaeoceanography of the North Atlantic and Tethys Oceans. Geol. Soc. Lond. Spec. Publ. 21, 299–320.
Roth, P.H., 1989. Ocean circulation and calcareous nannoplankton evolution during the Jurassic and Cretaceous. Palaeogeogr. Palaeoclimatol. Palaeoecol. 74, 111–126.
Roth, P.H., Bowdler, J., 1981. Middle Cretaceous nannoplankton biogeography and oceanography of the Atlantic Ocean. In: Warme, J.E., Douglas, R.G., Winterer, E.L. (Eds.), The Deep Sea Drilling Project: A Decade of Progress. SEPM. Sp. Publ. Vol. 32. pp. 517–546.
Roth, P.H., Krumbach, K.P., 1986. Middle Cretaceous calcareous nannofossil biogeography and preservation in the Atlantic and Indian Oceans: implications for paleoceanography. Mar. Micropaleontol. 10, 235–266.
Roth, P.H., Thierstein, H.R., 1972. Calcareous nannoplankton: Leg 14 of the Deep Sea Drilling Project. Initial Rep. Deep Sea Drill. Proj. 14, 421–485.
Sanei, H., Grasby, S.E., Beauchamp, B., 2012. Latest Permian mercury anomalies. Geology 40, 63–66.
Scarparo Cunha, A.A., Shimabukuro, I., 1997. *Braarudosphaera* blooms and anomalous enrichment of *Nannoconus*: evidence from Turonian South Atlantic, Santos Basin, Brazil. J. Nannoplankton Res. 19, 51–55.
Schlanger, S.O., Jenkyns, H.C., 1976. Cretaceous oceanic anoxic events: causes and consequences. Geol. Mijnb. 55, 179–184.
Schneidermann, N., 1977. Selective dissolution of recent coccoliths in the Atlantic Ocean. In: Ramsay, A.T.S. (Ed.), Oceanic Micropaleontology. Academic Press, New York, pp. 1009–1053.
Shannon, C.E., Weaver, W., 1949. The Mathematical Theory of Communication. University of Illinois Press (125 pp).
Stein, M., Westermann, S., Adatte, T., Matera, V., Fleitmann, D., Spangenberg, J.E., Föllmi, K.B., 2012. Late Barremian–Early Aptian palaeoenvironmental change: the Cassis-La Bédoule section, southeast France. Cretac. Res. 37, 209–222.
Street, C., Bown, P.R., 2000. Palaeobiogeography of early Cretaceous (Berriasian-Barremian) calcareous nannoplankton. Mar. Micropaleontol. 39, 265–291.
Suchéras-Marx, B., Giraud, F., Mattioli, E., Gally, Y., Barbarin, N., Beaufort, L., 2014. Middle Jurassic coccolith fluxes: a novel approach by automated quantification. Mar. Micropaleontol. 111, 15–25.
Tappan, H.L., 1980. The Paleobiology of Plant Protists. (San Francisco, 1028 p).
Taylor, K.G., Macquaker, J.H.S., 2000. Early diagenetic pyrite morphology in a mudstone-dominated succession: the Lower Jurassic Cleveland ironstone Formation, eastern England. Sediment. Geol. 131, 77–86.
Tejada, M.L.G., Suzuki, K., Kuroda, J., Coccioni, R., Mahoney, J.J., Ohkouchi, N., Sakamoto, T., Tatsumi, Y., 2009. Ontong Java plateau eruption as a trigger for the early Aptian oceanic anoxic event. Geology 37, 855–858.
Thierstein, H.R., 1980. Selective dissolution of Late Cretaceous and Earliest Tertiary calcareous nannofossils: experimental evidence. Cretac. Res. (2), 165–176.
Thierstein, H.R., Roth, P.H., 1991. Stable isotopic and carbonate cyclicity in Lower Cretaceous deep-sea sediments: dominance of diagenetic effects. Mar. Geol. 97, 1–34.
Tremolada, F., Erba, E., 2002. Morphometric analyses of Aptian Assipetra infracretacea and Rucinolithus terebrodentarius nannoliths: implications for taxonomy, biostratigraphy and paleoceanography. Mar. Micropaleontol. 44, 77–92.
Vail, P.R., Audemard, F., Bowman, S.A., Eisner, P.N., Perez-Cruz, C., 1991. The stratigraphic signatures of tectonics, eustasy and sedimentology - an overview. In: Einsele, G., Ricken, W., Seilacher, A. (Eds.), Cycles and Events in Stratigraphy. 1991. Springer-Verlag, Berlin, pp. 617–659.
van Breugel, Y., Schouten, S., Tsikos, H., Erba, E., Price, G.D., Sinninghe Damsté, J.S., 2007. Synchronous negative carbon isotope shifts in marine and terrestrial biomarkers at the onset of the early Aptian oceanic anoxic event 1a: evidence for the release of 13C-depleted carbon into the atmosphere. Paleoceanography 22, PA1210. https://doi.org/10.1029/2006pa001341.
Watkins, D.K., 1989. Nannoplankton productivity fluctuations and rhythmically-bedded pelagic carbonates of the Greenhorn Limestone (Upper Cretaceous). Palaeogeogr. Palaeoclimatol. Palaeoecol. 74, 75–86.
Watkins, D.K., Wise, S.W., Pospichal, J.J., Crux, J., 1996. Upper Cretaceous calcareous nannofossil biostratigraphy and paleoceanography of the Southern Ocean. In: Moguilevski, A., Whatley, R. (Eds.), Microfossils and Oceanic Environments. University of Wales, Aberystwyth Press, Aberystwyth, pp. 355–381.
Weissert, H., Erba, E., 2004. Volcanism, CO_2 and palaeoclimate: a Late Jurassic – Early Cretaceous carbon and oxygen isotope record. J. Geol. Soc. London 161, 1–8.
Weissert, H., Lini, A., Föllmi, K.B., Kuhn, O., 1998. Correlation of Early Cretaceous carbon isotope stratigraphy and platform drowning events: a possible link? Palaeogeogr. Palaeoclimatol. Palaeoecol. 137, 189–203.
Werner, R.A., Brand, W.A., 2001. Referencing strategies and techniques in stable isotope ratio analysis. Rapid Commun. Mass Spectrom. 15, 501–519.
Westermann, S., Stein, M., Matera, V., Fiet, N., Fleitmann, D., Adatte, T., Föllmi, K.B., 2013. Rapid changes in the redox conditions of the western Tethys Ocean during the early Aptian oceanic anoxic event. Geochim. Cosmochim. Acta 121, 467–486.
Wilkin, R.T., Barnes, H.L., 1997. Formation processes of framboidal pyrite. Geochim. Cosmochim. Acta 61, 323–339.
Wilkin, R.T., Arthur, M.A., Dean, W.E., 1997. History of water-column anoxia in the Black Sea indicated by pyrite framboid size distributions. Earth Planet. Sci. Lett. 148, 517–525.
Williams, J.R., Bralower, T.J., 1995. Nannofossil assemblages, fine fraction isotopes, and the paleoceanography of the Valanginian-Barremian (Early Cretaceous) North Sea Basin. Paleoceanography 10, 815–839.
Winter, A., Jordan, R.W., Roth, P.H., 1994. Biogeography of living coccolithophores in ocean waters. In: Winter, W.G. Siesser (Ed.), Coccolithophores. Cambridge University Press, pp. 161–177.
Wise, S.W., 1988. Mesozoic-Cenozoic history of calcareous nannofossils in the region of the Southern Ocean. Palaeogeogr. Palaeoclimatol. Palaeoecol. 67, 157–179.
Yamamoto, K., Ishibashi, M., Takayanagi, H., Asahara, Y., 2013. Early Aptian paleoenvironmental evolution of the Bab Basin at the southern Neo-Tethys margin: response to global carbon-cycle perturbations across Oceanic Anoxic Event 1a. Geochem. Geophys. Geosyst. 14, 1104–1130.